Designing and Vibration Analysis of a Transportable Reference Optical Cavity

A thesis
Submitted towards the partial fullfilment of
BS-MS dual degree programme
by

M Gautham Upadhyaya M

Date: 30.04.2024

under the guidance of

Supervisor: Prof. Subhadeep De, IUCAA

Co-supervisor: Prof. Sandip Haldar, IIT Goa

from May 2023 to April 2024

Indian Institute of Science Education and Research, Pune

Certificate

This is to certify that this dissertation entitled "**Designing and Vibration Analysis of a Transportable Reference Optical Cavity**" submitted towards the partial fulfillment of the BS-MS degree at the Indian Institute of Science Education and Research (IISER), Pune represents original research carried out by "**M Gautham Upadhyaya M**" at "**Inter-University Centre for Astronomy and Astrophysics (IUCAA), Pune**", under the supervision of "**Prof. Subhadeep De**", and co-supervised by "**Prof. Sandip Haldar (IIT Goa)**", during academic year May 2023 to March 2024.

Supervisor:
PROF. SUBHADEEP DE
ASSOCIATE PROFESSOR
IUCAA, PUNE

Co-supervisor:
PROF. SANDIP HALDAR
ASSOCIATE PROFESSOR
IIT, GOA

M GAUTHAM UPADHYAYA M
Roll No. 20191135
BS-MS
IISER Pune

Date: 30/04/2024

Declaration

I, hereby declare that the matter embodied in the report titled "**Designing and Vibration Analysis of a Transportable Reference Optical Cavity**" is the results of the investigations carried out by me at the "**Inter-University Centre for Astronomy and Astrophysics (IUCAA), Pune**" from the period 15-05-2023 to30-04-2024 under the supervision of **Prof. Subhadeep De**, and co-supervised by **Prof. Sandip Haldar** of IIT Goa, and the same has not been submitted elsewhere for any other degree. Wherever others contribute, every effort is made to indicate this clearly, with due reference to the literature and acknowledgement of collaborative research and discussions.

Supervisor:
PROF. SUBHADEEP DE
ASSOCIATE PROFESSOR
IUCAA, PUNE

Co-supervisor:
PROF. SANDIP HALDAR
ASSOCIATE PROFESSOR
IIT, GOA

M GAUTHAM UPADHYAYA M
Roll No. 20191135
BS-MS
IISER Pune

Date: 30/04/2024

Acknowledgements

I would like to express my heartfelt gratitude to Prof. Subhadeep De of IUCAA, Pune, and Prof. Sandip Haldar of IIT, Goa, for giving me the opportunity to work on this project and guiding me at every step. I have learned important lessons on research, ethics, and virtues from both of them, and feel grateful for their mentoring and patience. I also sincerely thank Prof. Shouvik Datta of IISER, Pune for his insights and constant support during my thesis.

I would like to thank the Director and administration of IUCAA, Pune for allowing me to carry out my thesis work at the institute and extending the campus facilities and resources. I am indebted to the Dept. of Science & Technology (DST), Govt. of India, via their Quantum Enabled Science and Technology (QuEST), and the Board of Research in Nuclear Science (BRNS) for the funding, and the I-HUB Quantum Technology Foundation at IISER, Pune for the student fellowship. I would also like to thank IIT, Goa for providing me with the computational facility required for the project.

I owe a huge thanks to my labmates at the Precision and Quantum Measurements Lab, IUCAA, Sankalpa Banerjee, and Dr. Stanley Johnson, for helping me out with the simulations, analysis, and resources, and for being ever available to clarify my doubts. To my other labmates who were a constant source of encouragement and support, Sankar Majhi, Dr. Sujaya Dasgupta, Arenjit Modal, and Venu Jangam - thank you for your kindness, and making this fun!

This journey would have been tough without the laughter, adventures, and countless cheerful moments that I shared with my friends. Thank you for being there for me. I am also grateful to my coach, Mr. Arvind Shastry, who I greatly admire for his immense support in my journey. And lastly, I would like to thank my family, who inspire me every day to do my best, and for always believing in me.

Abstract

A Fabry–Pérot cavity is widely utilized in multiple areas of physics, for mode-locking, spectroscopy, signal transmission, interferometers etc. Its use as a short-term optical reference is particularly relevant. Reference optical resonators can achieve exceptional frequency stability, and generate narrow line-width output, which is essential for a plethora of applications. In order to do so, they are isolated from each and every source of noise, and operated in a controlled laboratory setup. Today, there is an increasing demand for reference optical cavities that are portable, and also functional in a non-laboratory environment, without any loss in their stability or performance. Such reference cavities, for out of the lab uses, are called transportable Fabry–Pérot cavities.

The optical path length of the cavity is its absolute reference. The frequency instability of a Fabry–Pérot resonator is coupled to the relative length instability in the cavity. The length of the cavity, which is defined as the distance between the two reflecting surfaces, can vary due to temperature and pressure fluctuations, mechanical vibrations, acoustic noise, and even due to change of the gravitational acceleration, giving rise to permanent and dynamic deformations of the cavity. These external sources of noise are naturally more prevalent in non-laboratory conditions. Hence, developing a transportable Fabry–Pérot cavity that can maintain its stability in such conditions is extremely challenging.

The precise and robust design of a transportable cavity is a result of smart ideas, rigorous simulations and quantitative analysis. This is done to investigate the stability of the cavity under the influence of all possible external perturbations. The goal of this thesis is to design a transportable reference optical cavity for practical applications. The focus is on compactness, and developing a novel robust mount for the cavity, which is the most critical component in deciding the resonator stability. In the process, we also present in detail the procedures involved in the designing of a transportable Fabry–Pérot cavity. The significance of this study extends to developing transportable ultra-stable laser systems for portable optical clocks.

Contents

List of Figures

List of Tables

Chapter 1

Introduction

1.1 Fabry–Pérot cavity

A Fabry–Pérot cavity (or a Fabry–Pérot etalon, often abbreviated as an FP cavity) is an optical resonator formed by the configuration of two mutually facing reflecting surfaces, or mirrors, separated by a distance. Unlike a Fabry–Pérot interferometer, which also comprises of two mutually facing mirrors, a spacer is used in a Fabry–Pérot cavity to enclose the distance between the mirrors 1.1. A few typical FP cavity geometries are shown in Fig.1.2. In the present day, Fabry–Pérot cavities are ubiquitously employed in the field of optics, atomic physics, and precision metrology that require a frequency reference with stability ranging from 10^{-14} to 10^{-17} and beyond for various applications.

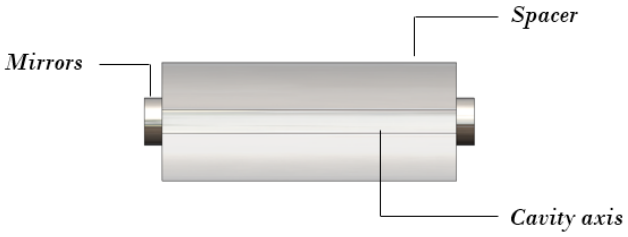

Figure 1.1: Fabry–Pérot cavity comprising a spacer, and two mirrors attached to its ends.

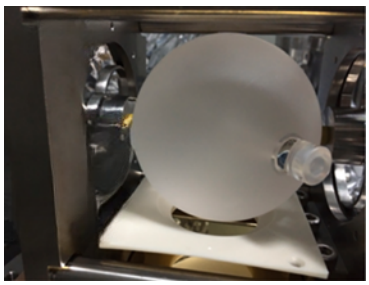

(a) $d = 78$ mm Sphere [1]

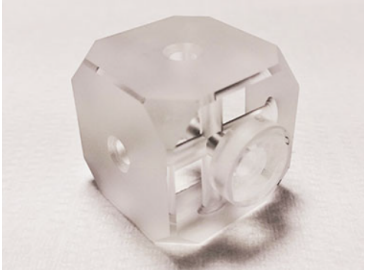

(b) $s = 50$ mm Cube [2]

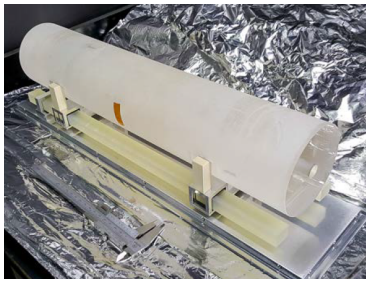

(c) $l = 485$ mm Cylinder [3]

Figure 1.2: Fabry–Pérot cavities of different length and spacer geometries.

1.1.1 Cavity response and key properties

The fundamental treatment of Fabry–Pérot resonators, commonly found in textbooks [4], relies on a geometric multiple-beam interference model. Here, the resonator is depicted as plane parallel mirrors separated by distance L and a medium of refractive index n. This intuitive approach, which considers input excitations of constant amplitude, suffices to explain the static behaviour of the cavity. From this method, key properties such as the resonance condition, cavity free spectral range, line-width etc. can be derived. A more advanced approach based on differential equations is required to describe input excitations with time-varying amplitudes [5]. In addition, this method assumes cavity length and input laser frequency to be constant.

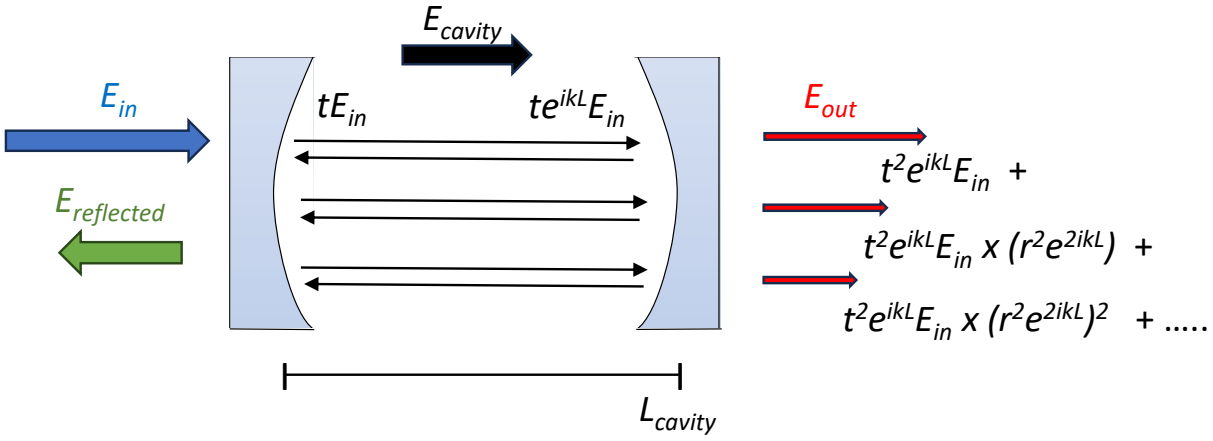

Figure 1.3: Schematic representation of the inter-cavity field build-up and cavity response.

A monochromatic input optical field at frequency ω and wave vector $\mathbf{k}$ can be represented using the equation:

$$E_{in} = E_0 e^{i(kz-\omega t)} \tag{1.1}$$

When the plane wave illuminates the first mirror, depending on the reflectivity of the mirror 1.3, the field is partially transmitted and partially reflected. Assuming normal incidence, the filed amplitude that enters the cavity is simply tE_{in}, where, t is the amplitude transmission coefficient. The relation between t and r, amplitude reflection coefficient, is governed by Fresnel equations:

$$t^2 = (1 - r^2) \quad \text{or} \quad T = 1 - R \qquad \text{where} \quad T = t^2 \quad \& \quad R = r^2 \tag{1.2}$$

As the field inside the cavity travels the length L, it gains an additional phase of e^{ikL} (we assume n=1 for simplicity). The field encounters the second mirror and undergoes

reflection and transmission similar to the first interface. The amplitude of transmission from the second mirror becomes:

$$E_{out1} = t^2 e^{ikL} E_{in} \tag{1.3}$$

The reflected wave from the second mirror travels back, and the process of reflection and transmission repeats. Each time the wave reaches the second mirror after covering twice the cavity length, a phase of e^{2ikL} gets added. Considering the amplitude reflection coefficient r, we get the successive transmission amplitudes due to multiple reflections as:

$$\begin{aligned} E_{out2} &= t^2 e^{ikL} E_{in} (r^2 e^{2ikL}) \\ E_{out3} &= t^2 e^{ikL} E_{in} (r^2 e^{2ikL})^2 \\ E_{out4} &= t^2 e^{ikL} E_{in} (r^2 e^{2ikL})^3 \end{aligned} \tag{1.4}$$

and so on.....

The cavity output field is the summation of all the amplitude components, and takes the form of a geometric sum. The cavity transmission coefficient T_{cav}, and reflection coefficient R_{cav}, expressed just in terms of r (the mirror reflection coefficient), can be obtained as:

$$T_{cav} = \frac{E_{out}}{E_{in}} = \frac{(1-r^2)e^{ikL}}{1-r^2 e^{2ikL}}; \qquad R_{cav} = \frac{r(e^{2ikL}-1)}{1-r^2 e^{2ikL}} \tag{1.5}$$

The static amplitude and phase of the resonator are entirely characterised by R_{cav} and T_{cav}. Finally, we define the transmission intensity response function, otherwise known as the cavity transmittance, as $\mathbb{T} = |T_{cav}|^2$, which follows the *Airy distribution* function.

$$\mathbb{T} \equiv |T_{cav}|^2 = \frac{1}{1 + \frac{4r^2}{(1-r^2)^2}\sin^2(kL)} \tag{1.6}$$

This function peaks for $kL = m\pi$, where m is a positive integer. Since, k can be expressed as $2\pi/\lambda$, the condition can be reframed as $2L = m\lambda$. The transmission peaks essentially due to the constructive interference inside the cavity leading to a large inter-cavity field, and the cavity is said to have attained *resonance*. The resonance condition in terms of input frequency ν is:

$$\nu = m\frac{c}{2L} \qquad \text{or} \quad \nu = m\frac{c}{2nL} \quad \text{in general} \tag{1.7}$$

with n being the refractive index of the medium between the mirrors. These frequencies are called the **resonant modes** of the cavity. The Free Spectral Range (FSR) of the cavity is defined as the frequency spacing between two adjacent resonant modes of the

cavity. Typical FP cavities of few cm in length have FSR in the range of MHz to GHz.

$$\Delta\nu_{FSR} = \frac{c}{2nL} \tag{1.8}$$

The full width at half maximum (FWHM) of the resonance peaks is the cavity line-width $\Delta\nu_{FWHM}$ (The approximation applied in order to obtain the line-width from 1.6 is valid for r close to 1).

$$\Delta\nu_{FWHM} \approx \frac{c}{2\pi nL}\frac{(1-r^2)}{r} \tag{1.9}$$

The cavity *finesse* ($\mathcal{F}$) is the ratio of peak separation (FSR) to peak width (or cavity line-width). This definition also forms the basis for experimentally determining the reflectivity of mirrors, and thereby their finesse, with high accuracy using optical feedback in the ring-down measurement technique [6]. The finesse of the cavity depends only on the reflectivity of the mirrors:

$$\mathcal{F} \approx \frac{\Delta\nu_{FSR}}{\Delta\nu_{FWHM}} = \frac{\pi r}{(1-r^2)} \tag{1.10}$$

Fig.1.5 shows the increasing finesse for cavity with mirrors of higher reflectivity, R. For a cavity of given length, a higher finesse results in the narrowing of the line-width, as shown in Fig.1.4 & 1.6. This feature allows one to use the FP resonator for mode-locking or as a mode discriminator. At high reflectivity ($R \geq 0.9$) the frequency spectrum of the cavity approaches a Lorentzian profile. A detailed account on the cavity response, spectral line shapes, finesse, intensity etc. can be referred from [5, 7].

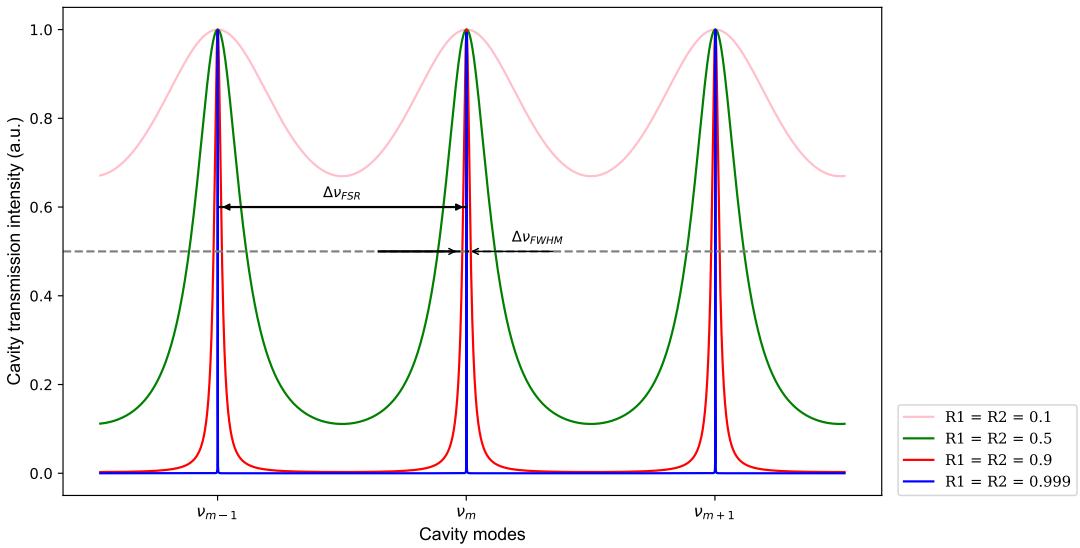

Figure 1.4: Cavity transmission intensity for various mirror reflectivity. The cavity line-width narrows as the reflectivity (or finesse) goes higher.

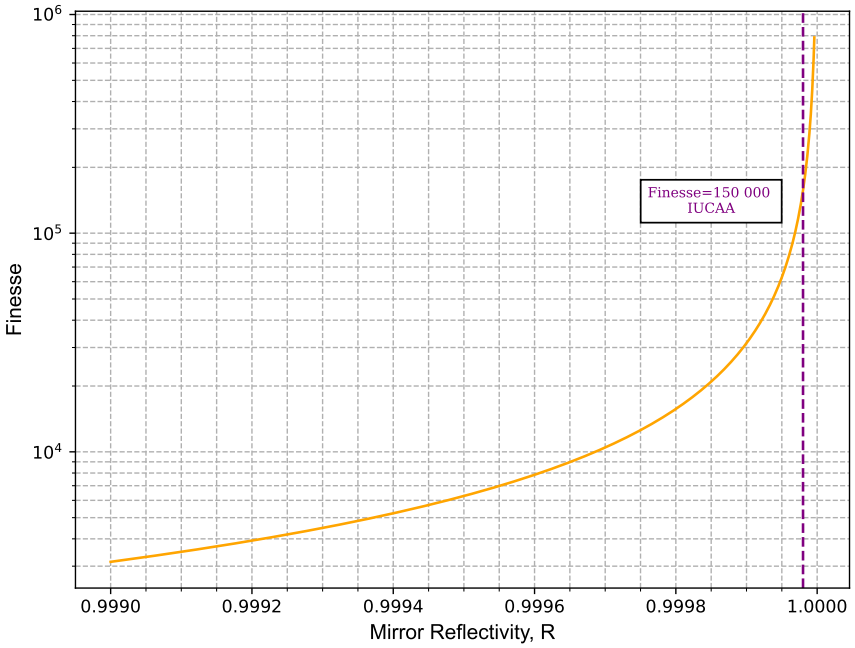

Figure 1.5: Cavity finesse for increasing mirror reflectivity $R_1 = R_2$. The plot also shows the finesse of the cavity used for the laboratory-based cavity at IUCAA.

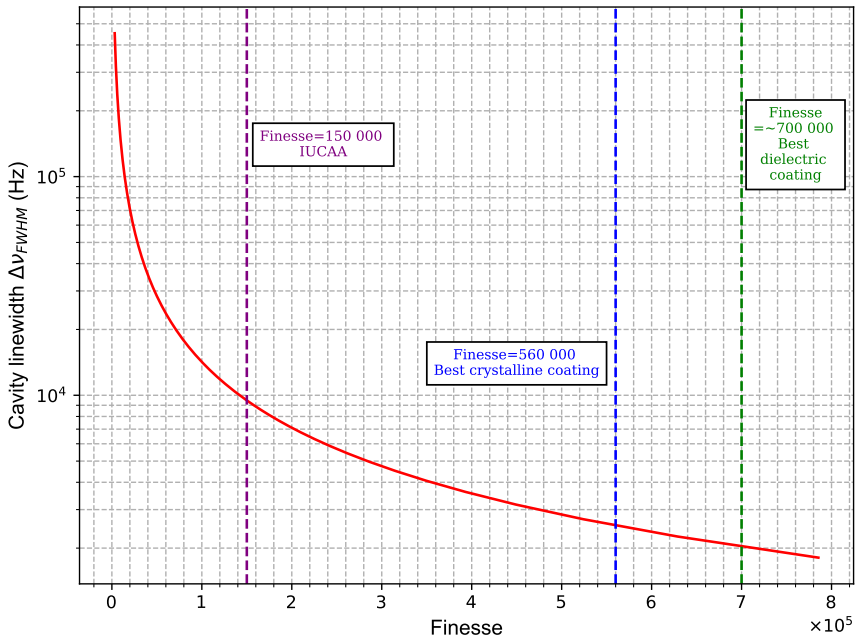

Figure 1.6: Cavity line-width for increasing mirror finesse. The plot also shows the best finesse obtained for dielectric and crystalline mirrors till date.

One of the most preferred methods to lock a free-running laser to an FP cavity is the Pound-Drever-Hall (PDH) method [8], in which the intensity of the reflected light from the cavity is held to zero as the reference for feedback. The derivative of the reflected intensity, is anti-symmetric about resonance. Measuring this derivative, one would have an error signal that can be used to lock the laser.

It is useful to maximize the slope of the error signal for an efficient PDH locking [9]. This slope is a measure of the sensitivity of the error signal to fluctuations in the laser frequency (or cavity length). One example of when this a high sensitivity in the slope/discriminant is required is if one needs a large gain in the feedback loop. The slope depends on the cavity finesse, the laser wavelength, and the power in the side bands and the carrier. Cavities with a higher finesse are more efficient simply because they enhance the sensitivity of the PDH error signal to the resonance frequencies, and hence perform the best locking. This is demonstrated in Fig.1.7 which shows the increasing sensitivity of the cavities to the PDH locking for increasing cavity finesse. This is the reason why higher finesse is preferred for FP cavities.

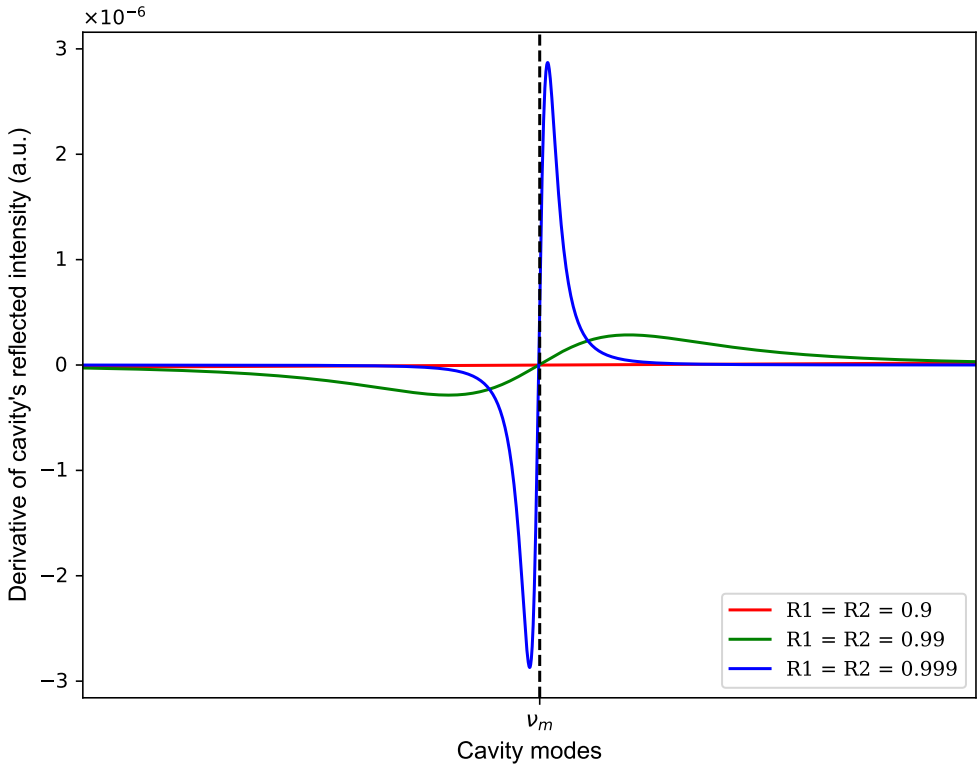

Figure 1.7: The derivative of the reflected intensity in cavity showing higher sensitivity for cavity with higher reflectivity, a.k.a finesse.

1.1.2 Stability phase diagram

A stable Fabry–Pérot resonator is one in which the photons resonate inside the cavity without any optical loss. In a dual-mirror linear cavity, this is achieved for certain configurations of mirrors with appropriate radii of curvature. The combination of values for the radius of curvatures of the two mirrors that can attain the geometric stability for a cavity is represented through a stability-phase diagram (Fig. 1.8) [10]. The geometric

stability criterion is defined by $0 \leq \sqrt{(\mathcal{G}_1\mathcal{G}_2)} \leq 1$. $\mathcal{G}_1$ and $\mathcal{G}_2$ are related to the radius of curvature as $\mathcal{G}_1 = (1 - \frac{L}{R_1})$ and $\mathcal{G}_2 = (1 - \frac{L}{R_2})$, where R_1 and R_2 are radii of curvatures of the two mirrors. The entire coloured region corresponds to the values of $\mathcal{G}_1$ and $\mathcal{G}_2$ that satisfy the **stability criterion**.

A commonly used mirror configuration in Fabry–Pérot resonators is the hemispherical cavity, where a concave mirror with radius of curvature of few meters is put together with a plane mirror (ROC $= +\infty$). Certain mirror configurations on the edges of the stability diagram are leveraged for sensor applications, as discussed in the next section.

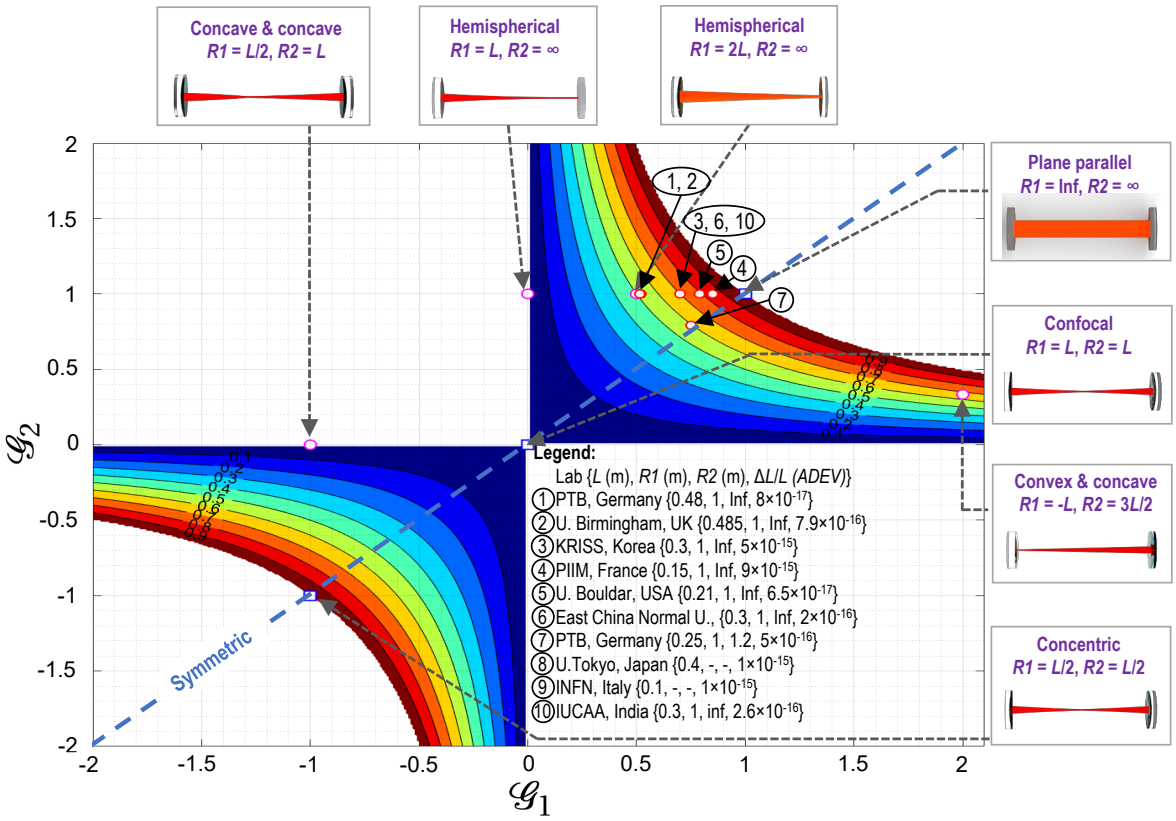

Figure 1.8: Stability phase diagram of the Fabry–Pérot resonator [10].

1.2 Optical reference vs sensor

Previously, we defined the free spectral range of a Fabry–Pérot cavity. The resonant modes of a cavity are integral multiples of the fundamental cavity mode ($m = 1$):

$$\nu = m\frac{c}{2nL} = m\Delta\nu_{FSR} \tag{1.11}$$

Assuming vacuum ($n = 1$), which can be reasonably achieved inside a cavity, and differentiating the eq.1.11 we obtain,

$$\frac{\Delta\nu}{\nu} = \frac{-\Delta L}{L} \tag{1.12}$$

where $\Delta\nu$ is the frequency noise of the cavity, and ΔL is the the change in cavity length. The above equation establishes a *frequency to length relation* in a Fabry–Pérot cavity. The noise or the instability in the frequency domain is coupled to the instability in cavity length. In other words, the length of the cavity can be taken as a reference, and fed back to the laser in order to achieve frequency stabilization. This lays the foundation for a short-term optical reference. By precisely controlling the length of the cavity, we can in turn achieve a stable narrow line-width output. However, this means the cavity has to be isolated from the factors which can perturb its length, including temperature fluctuations, mechanical vibrations, variations in acceleration due to gravity, acoustic noise etc. A cavity specifically designed to mitigate these noises in order to obtain a very low relative length instability is known as an **Ultra-stable Fabry–Pérot cavity** [11, 12]. These cavities act as short-term reference optical resonators.

An ultra-stable FP cavity can be used to generate a highly stable narrow line-width frequency reference [13]. When a commercial laser with MHz line-width is locked to an ultra-stable reference cavity, it can produce a sub-Hz line-width output, corresponding to a frequency instability of $\leq 10^{-15}$. This is utilized in optical clocks, which require the kind of stability to measure time at an unprecedented precision of 10^{-18} in long-term [14]. The lowest noise lasers are realized by stabilizing laser frequency onto an ultra-stable cavity of high finesse using the Pound–Drever–Hall (PDH) method [8]. Such ultra-stable lasers are used for atom interferometry [15], qubit control in quantum computing [16], microwave generation for RADAR applications [17], and in testing theories of relativity and dark matter [18, 19].

Fabry–Pérot sensors:

A stable cavity impervious to external conditions, can also be exploited for sensing applications. A sensor is any device which is sensitive to the change in the parameter it is supposed to measure, or detect. Many sensors that we use today like the MEMS accelerometers, fibre-based pressure and temperature sensors, gravitational wave detectors operate on the principle of Fabry–Pérot interferometers. A traditional interferometer has both or at least one of the mirrors free-moving or suspended, contrary to the rigidly fixed mirrors of a cavity. Hence, an unconventional approach is suggested for cavities to be used with mirror configurations that lie on the edges of the stability-phase diagram. Such cavities are called as **Near Unstable Cavities (NUC)**. Cavities operating in the

near unstable regime can be tipped off the stability region from the slightest of length fluctuations or mirror distortions. This makes them extremely sensitive detectors. Near concentric mirror configurations ($\mathcal{G} > 0.98$) also have the ability to enhance the thermal stability limit of the cavities.

The behaviour of NUC substantially deviates from the usual stable Fabry–Pérot cavity and accounts for additional complications arising due to beam interactions, mirror imperfections etc, but do not rule out the possibility of effective sensors entirely. Alvarez, MD [3] presents a detailed analysis and a few preliminary results in developing an advanced gravitational wave detector using near unstable cavities.

1.3 Lab-based Fabry–Pérot cavities

A stable Fabry-Pérot cavity in the form of an optical resonator or optical reference has wide-range applications in diverse fields. The design and requirements of a cavity can vary according to its working environment. FP cavities are extensively used in a controlled laboratory conditions for different purposes. In an atomic physics laboratory, a cavity stabilized laser is essential for studying the light-matter interactions, laser cooling techniques, and understanding various processes including but not limited to photoionisation, spectroscopy and the behaviour of atoms in different conditions. In metrology, ultra-stable narrow line-width frequency generation is critical for time and frequency standards. Ultra-stable cavities are an essential component of optical clocks, and are a pre-requisite in developing interrogation lasers for the clock reference transitions [20]. Trapped ions (for e.g., $^{171}Yb^{+}$) being one of the leading candidates for qubits, a compact laser system for manipulating its quantum states have proven highly effective [16]. Cavities are also important in enabling several experiments of fundamental interest, testing the validity of Lorentz invariance [21], time constancy of fundamental constants etc.

A complete laser system involves the laser source (diode laser, fibre laser etc.), a stable Fabry–Pérot resonator, servo locking electronic hardware, photodiode, and optical and electronic noise cancellation equipment. In a standard laboratory, this can be spaciously laid out on an optics table. The thermal stability of the cavity is taken care by multiple layers of thermal shields, and an active temperature control. The cavity along with its thermal shields is placed inside a vacuum chamber with ultra-high vacuum. And finally, the cavity chamber is kept over an active vibration-isolation table which cancels out the mechanical vibrations caused due to the seismic activity.

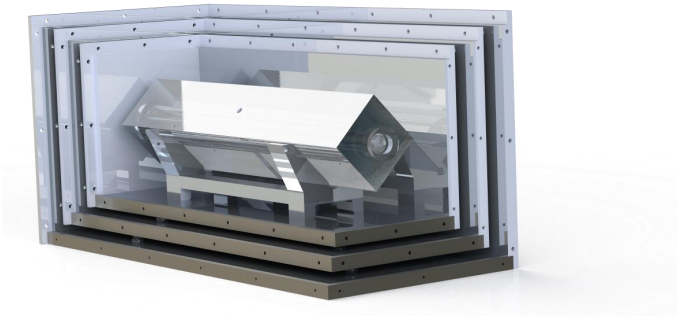

Figure 1.9: 3D rendered image of a 29.5cm lab-based ultra-stable Fabry–Pérot cavity with thermal shield layers, designed at PQM lab, IUCAA [10].

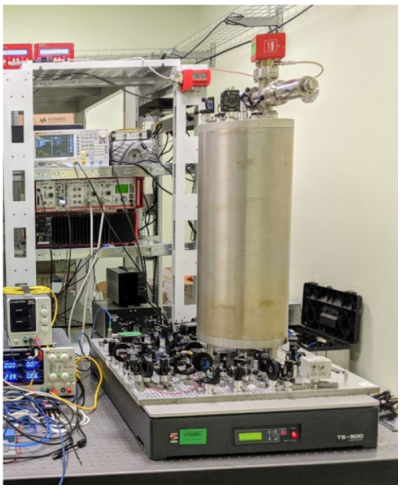

Figure 1.10: Lab set-up of a 48cm long vertically mounted room-temperature cavity on an optical breadboard [22].

The lab-based FP cavity can be operated at room-temperature [23], or using cryogenics [24] in order to reduce the thermal noise arising due to the Brownian motion in the mirror substrate and coating substances. **Cryogenic cavities** are feasible in a laboratory since one can afford the extra power requirements and bulk machinery. The state-of-the-art monolithic cryogenic Fabry–Pérot cavities made from silicon spacer and crystalline mirror coatings have achieved some of the best frequency stabilities till date with ADEV of 4×10^{-17} [25], 1×10^{-16} [26], and 3.5×10^{-17} [27] at short-term.

1.4 Transportable Fabry–Pérot cavities

In this section, a working definition for a Transportable Fabry–Pérot cavity along with its primary requirements are presented. The applications of transportable cavities are discussed, which highlights their significance. Further, the existing transportable cavity designs and their achieved stability is reviewed.

While it is ideal to operate a cavity in laboratory conditions, not all circumstances and experiments are situated or facilitated inside a laboratory. In such scenarios, one is obliged take measurements that are specifically in a non-laboratory environment, or carry out an entire experiment that is possible only outside the laboratory: on land or even in space.

This demands a different kind of Fabry–Pérot cavity that can be carried outside the laboratory or even be moved multiple times. More importantly, the cavity should not be affected or disoriented due to vibrations and handling during packing (and unpacking),

lifting, transport etc. The cavity needs to withstand the non-laboratory environment, yet not compromise its performance. For practical purposes, the cavity needs to be integrated with the its laser and the essential electronics, with the entire set-up being rigid and compact. Lastly, due to presumable absence of optics table at every location and for transport convenience, the cavity assembly should be mountable on a commercial rack. The above features define a Transportable Fabry–Pérot cavity. We can conceptualize a transportable cavity using the following description:

"**A transportable cavity is characterised by its stable & robust mounting, which allows it to maintain its integrity during the course of transport. After transport, the cavity should operate at the same stability as it was before the transport**."

In a laboratory, it is sufficient for the cavity to be just placed over support points which cause minimum deformation due to self-weight (such points are called Airy points). However, for a transportable cavity, the supports have to firmly hold the cavity so that it is not displaced or disoriented during transportation. Thus, the mounting structure for a transportable cavity have to satisfy additional criteria:

Mounting requirements:

→ **The cavity mounting is rigid and compact**.

→ **Motion is constrained in all directions (translation and rotation)**.

→ **Sustain Acceleration & Vibrations during transport**.

→ **Minimum deformation due to support/compressive forces**.

1.4.1 Applications

Transportable Fabry–Pérot cavities are becoming increasingly relevant in advancing physics and technology. In upgrading optical clocks to portable optical clocks, transportable ultra-stable FP cavities are essential as short-term frequency references. Such optical clocks will not only help us realize the redefinition of time with improved precision, but also enable advances in metrology which weren't feasible until now. For instance, geodesic mapping of the earth surface has been a long-standing goal of science. With accurate geodic measurements made possible by portable clocks, one can hope to achieve the mapping. Attempts to develop interrogation laser systems for transportable lattice-based Sr clocks, Yb^+ clocks, Ca^+ clocks for various applications are already on the go [28–30].

Ultra-stable lasers can have their utility extended to radio frequency (RF) and microwave frequencies through the technique of optical frequency division (OFD) [31], which can result in improved RADAR technology, 6G communication, as well as high speed quantum communication, namely the Twin field-Quantum Key Distribution (TF-QKD) [32]. The present-day navigation satellites are synchronised using microwave atomic standard frequencies. Replacing them with optical frequency standards improves navigation accuracy for military and everyday applications [33].

In the coming decades, many advanced physics experiments in hope of discovering new phenomena are aimed to be carried out in space. Laser Interferometer Space Antenna (LISA) is one such ambitious project for low frequency gravitational wave detection [34]. A set of three satellites separated by millions of kilometres sending laser beams at each other forms a huge interferometer in detecting faint gravitational waves. A more sophisticated form of transportable lasers which are space-grade play a pivotal role in development of such next-generation gravitational wave detectors [35]. Apart from gravitational waves, several exciting experiments for the detection of dark matter, Lorentz Invariance violation etc. have also been proposed with the help of space-grade transportable cavities [36, 37].

Table 1.1: Fractional frequency stability achieved by some of the state-of-the-art Fabry–Pérot cavities

Type of cavity	Allan Deviation at short-term
Lab-based Room-temperature	8×10^{-17} [38]
Lab-based Cryogenic	4×10^{-17} [25], 3.5×10^{-17} [27]
Transportable	1.6×10^{-16} [38], 2×10^{-16} [39]
Transportable Space-grade	4.2×10^{-16} [40]

1.4.2 Available transportable FP cavities

In the last decade, major advances have been made in the development of transportable Fabry–Pérot resonators for enhancing their stability and optimising for specific applications. Although the developments in lab-based room-temperature cavities and transportable cavities have gone hand-in-hand, they have often been motivated by clearly different goals. Cavities of different sizes and shapes, with a range of material compositions and structural aspects have been tested and improvised. The stability of the cavities ultimately depends on the length fluctuations, which is predominantly affected

by temperature fluctuations and mechanical vibrations. In a laboratory environment, the vibrations can be greatly suppressed and therefore, a simple mounting is effective. Lab-based ultra-stable cavities are thermally-limited, meaning, the instability due to thermal fluctuations dominate. The development of lab-based cavities primarily focuses on different materials and techniques that can reduce the thermal noise. On the contrary, transportable cavities are vibration-limited due to the elevated vibration levels, and a higher coupling between the cavity and seismic vibrations. Hence, the motivation for improved transportable cavity designs lies towards seeking novel spacer geometry and suitable support structures to suppress the mechanical vibrations.

To achieve a higher vibration stability, different spacer geometries like spherical cavities, cubical cavities, cuboidal cavities, cylindrical cavities with horizontal and vertical orientations, and other special geometries have been employed. It is noted that the support structures adopted are purely geometry-specific, and do not provide any universal mounting strategy. Moreover, these ideas are arrived at intuitively, and their optimization is perhaps, a result of a large number of modelling and trial simulations. The stability of different cavities also does not exhibit favouritism towards any particular cavity geometry, as shown in the Fig.1.11.

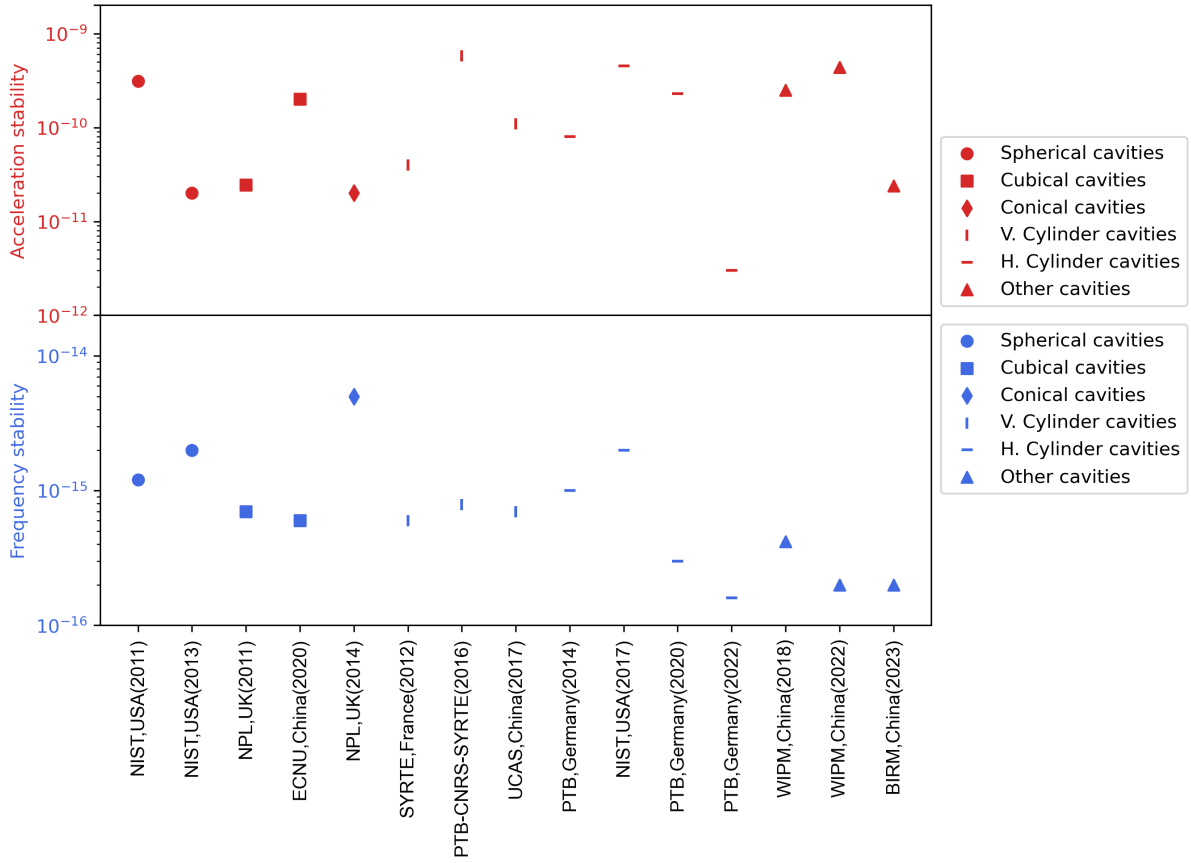

Figure 1.11: Comparison of stability of the transportable FP cavities designed by different groups. The "other cavities" correspond to special geometries mentioned in table 1.2

Table 1.2: Some of the available transportable cavities and their features.

Sl. No.	**Lab/Group**	**Spacer length (in mm)**	**Geometry**	**Size, Weight and Power (SWaP)**	**Stability (ADEV at 1 sec)**	**Application**
1	NIST, USA (2011) [41]	50.8	Spherical	$60 \cdot 45 \cdot 30$ cm^3 34 kg -	1.2×10^{-15}	Synthesis of low-noise RF or microwave signals
2	NPL, UK (2011) [42]	50	Cubical	No sufficient information	7×10^{-16} Ref.	For use in non-laboratory environments
3	UCAS, China (2022) [43]	100	Cubical	$10 \cdot 10 \cdot 10$ cm^3 (cavity spacer) - 55 µW	-	Ultra-stable laser systems for space applications
4	NPL, UK (2014) [44]	100	Conical	0.3 m^3 50 kg 12 dBm	5×10^{-15}	Optical carrier frequency transmission in fibre networks
5	SYRTE, France (2012) [45]	100	Vertical cylinder	$17 \cdot 30$ cm^3 (cylindrical vacuum chamber) 40 kg (cavity assembly) 15 mW	6×10^{-16}	Developed as a part of PHARAO space clock project
6	PTB, CNRS, SYRTE etc. (2016) [46]	100	Vertical cylinder	$30 \cdot 30 \cdot 30$ cm^3 (cavity + vacuum chamber) $60 \cdot 45 \cdot 8$ cm^3 (optics module) - 1.5 µW	7.9×10^{-16}	Developed towards interrogation laser system for a Sr lattice clock within Space Optical Clock2 (SOC2) project

7	NIST, USA (2017) [47]	25	Horizontal cylinder	61 cm^3 (cavity assembly) - 70 µW	2×10^{-15}	Reference cavity for photonic microwave generation system
8	PTB, Germany (2020) [48]	120	Horizontal cylinder	27 ·19 ·20 cm^3 8 kg -	3×10^{-16}	Interrogation laser system for a transportable Sr lattice clock
9	PTB, Germany (2022) [49]	200	Horizontal cylinder	- - 10 µW	1.6×10^{-16}	Transportable clock laser system
10	WIPM; UCAS, China (2022) [39]	300	Cuboidal	48 · 26.5 · 23 cm^3 41 kg -	2×10^{-16} Line-width: 0.14Hz	Reference lasers for optical frequency comparison and conversion stations
11	FEMTO-ST, France (2018) [50]	25	Tetrahedral	3.5 · 3.6 · 4.1 cm^3 (cavity) 30 L (optical setup)	7.5×10^{-15}	Ultra-compact laser system
12	BIRM, China (2023) [51]	30	"Lantern"	No sufficient information	2.0×10^{-16} (simulated result)	Miniature transportable optical reference cavity

To achieve a higher vibration stability, different spacer geometries like spherical cavities, cubical cavities, cuboidal cavities, cylindrical cavities with horizontal and vertical orientations, and other special geometries have been employed. It is noted that the sup-

port structures adopted are purely geometry-specific, and do not provide any universal mounting strategy. Moreover, these ideas are arrived at intuitively, and their optimization is perhaps, a result of a large number of modelling and trial simulations. The stability of different cavities also does not exhibit favouritism towards any particular cavity geometry, as shown in the Fig.1.11.

While no design is perfect, each design stands unique and offers perspectives on mounting techniques and scope for future improvement. The following is a brief account of some of the note-worthy transportable cavity designs devised by groups across the world, in more or less a chronological order:

The most natural and simple geometry for a Fabry–Pérot cavity, is a cylindrical spacer with the mirrors fixed to both ends. It was, and still is widely used for lab-based cavities. A simple four-point symmetric mounting with minimal deformation works efficiently for a laboratory cavity [52], but the mounting is not rigid enough for transportable purposes. Using a symmetric rigid mounting on a cylindrical spacer without causing serious deformations is non-trivial. Leibrandt et. al. of NIST, USA [41] and Webster & Gill from NPL, UK [42] were one of the first groups to deviate from the traditional cylindrical geometry and explore other possibilities for a transportable cavity. The former adopted a spherical spacer with two-point symmetric mounting, while the later opted for a cubic spacer with a mounting that had a tetrahedral symmetry. The support structures in a transportable cavity generally apply a compressive force to rigidly withhold the cavity. These forces affect the cavity length. The mounting designed by the two groups relied on the principle of symmetric cancelling of the mounting forces in such a manner that, the deformation along the length of the cavity due to the mounting forces is near zero. Both the cavities provide great stability, with the cubic cavity being more preferred due to its compactness and higher tolerance. Cubic cavities are extensively used, demonstrating high stability and even space-grade compatibility [43, 48, 53].

Design challenge1: Larger cavity volume for a given length scale. Transportable applications prefer smaller cavity size and light-weight.

The most commonly seen geometry amongst the transportable FP resonators is the cylindrical spacer, but with modifications or spacer appendages. Cylindrical cavities can be mounted vertically, or horizontally. Accordingly, two major kinds of modifications are widely observed. The first kind involves a mid-planar concentric ring, or a collar, attached to the spacer. Vertically mounted cylindrical cavities predominantly adopt this modification. The collar allows for a mounting that effectively decouples the mounting forces from the cavity length. Of all the cylindrical cavities with vertical orientation, the one developed by Argence et. al. (SYRTE, France), which uses a special Cavity Fastening Device (CFD), offers better thermal and vibration stability compared to other mounts

[45]. The second type of modification is pioneered by PTB, Germany, for horizontal cylindrical (and also cuboidal) spacers. The design utilizes a twelve-point mounting to constrain the cavity's motion in the three directions [54]. The technique is based on decoupling the mounting forces from each other, via independent supports for each degree of freedom. This greatly improves the vibration stability. This design has been perfected to obtain the most stable transportable Fabry–Pérot cavity till date, achieved by Sophia et. al. of PTB, Germany [49].

Design challenge2: Complex mounting techniques. Design of the mounting structures are intricate, and demand skilled manufacturing and assembling.

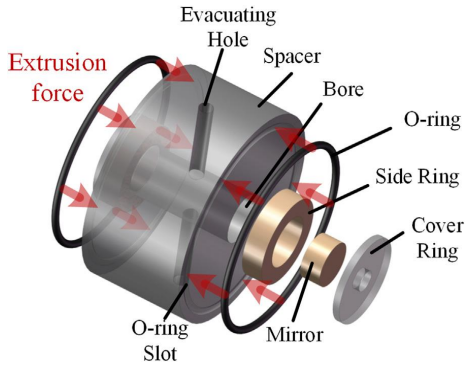

(a) 3cm "Lantern cavity" proposed by BIRM, China, for tuneable thermal properties [51].

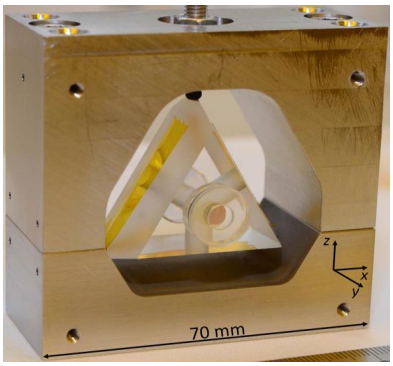

(b) 2.5cm ultra-compact cavity with tetrahedral spacer, developed by FEMTO-ST, France [50].

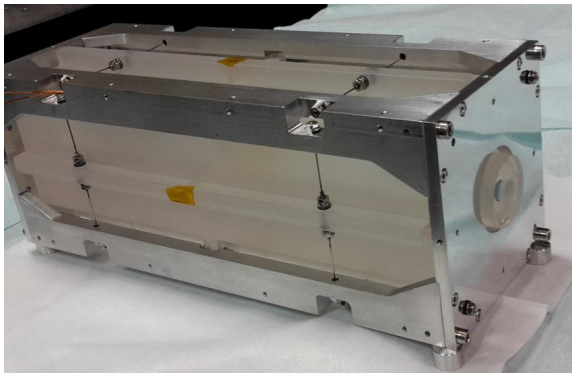

(c) 20cm Horizontal cylindrical cavity by PTB, Germany with highest achieved stability amongst transportable cavities [49].

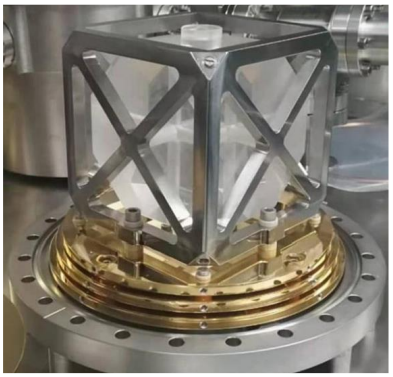

(d) 10cm Cubic cavity mounted on a bracket with tetrahedral symmetric support, built by NTSC, China [55].

Figure 1.12: Transportable cavity designs with different spacer geometries and geometry-specific mountings.

The other broad category of transportable cavity designs employs special modified geometries, either derived from a basic geometry, or was optimised to enhance the vibration stability. Some of the cavity designs considered under this category include tetrahedral spacer, conical/tapered cylinder spacer, and modified cylinder/"lantern" spacer. The most notable feature about these designs is their miniature size. Smaller and less bulkier cavities are more suited for transportable designs. The tetrahedral design with a three-point mounting is ultra-compact, with a cavity length of 25 mm [50]. The conical spacer design was adopted by JPL, NASA for space-grade cavities [56], and was also harnessed by NPL, UK [44] for optical frequency transmission experiments. The lantern spacer, first developed by FEMTO-ST, France, is in fact a cylindrical spacer with large diameter-to-length ratio [47]. It is also a miniature cavity of 25 mm length. A very recent article by BIRM, China proposed to integrate a re-entrant mirror structure with this geometry for tuneable thermal property in cavities [51].

Design challenge3: Spacer machining is highly specialized. ULE is an expensive material and not easily accessible. High quality machining and polishing of ULE glass required for cavities is challenging.

1.5 Goals and scope of this project

The objective of this work is to design a compact transportable reference optical cavity for out of the lab applications. For convenient transport and operation, the cavity is designed in such a manner that it is rack-mountable, and is integrated along with its optics module and servo electronics within a single commercially available 19" rack.

In order to achieve the required frequency stability, all the sources of optical, electronic and thermo-mechanical noise are carefully analysed. Transportable cavities are highly susceptible to the mechanical vibration noise. Hence, this work is primarily dedicated towards addressing the vibration noises in the cavity. To overcome this, novel spacer geometries and mounting techniques are explored with an aim to make the cavity robust for non-laboratory conditions. This is achieved through smart and efficient cavity mounting designs, and meticulous computational analysis in the form of Finite Element simulations. Specialised simulation software are employed for the purpose.

The targeted vibration stability for the transportable cavity in terms of $\frac{\Delta L}{L} \cdot g^{-1}$ is $\leq 10^{-10}$, which can be expected to offer a fractional frequency stability of $\mathcal{O}(10^{-16})$ at short-term. The stability achieved through simulations are tried to hit higher than the required threshold, in consideration of the tolerances in machining process, and inevitable inaccuracies during mounting and assembly.

The complete design of a transportable cavity necessarily involves elaborate vibration and thermal analysis. In cognizance of the time constraint, only vibration analysis has been carried out. The completion of the the cavity design is subject to further thermal analysis and designing of suitable thermal shields and vacuum chamber, which is not a part of this thesis.

Chapter 2

Methodology

This Chapter provides a detailed perspective at the approach towards designing a transportable Fabry–Pérot cavity, and the critical aspects to consider in the process. Different sections of the Chapter will elaborate on the step-by-step procedure followed in designing the cavity to achieve required stability. The challenges and limitations at every stage are also discussed in order for the reader to appreciate the merits and demerits.

2.1 Overview of the cavity designing process

The designing of a transportable cavity is a multi-physics problem accounting for optics, thermo-mechanics, and manufacturing aspects. The process is based on understanding the role of different external influences on its stability through modelling, simulations, and analysis. Before discussing the motivation behind them, one needs to understand the different aspects of designing a transportable cavity for making strategic design choices. The following are the critical features in the design of a transportable FP cavity:

1. **Length of the cavity**: The very first thing that is addressed in the designing process is the length of the cavity. Based on the application and the compactness required, the spacer length is decided using the *frequency to length* relation (eq. 1.12). This step precedes the rest because the assembly size scales according to the length scale.

2. **Geometry of the spacer**: Once the length is finalised, a suitable shape for the spacer is opted. This step involves analytics and modelling in choosing an optimum geometry. The decision is also influenced by the application in consideration. Geometry of the spacer is very crucial, since the mounting techniques are generally geometry-specific, and ultimately determine the thermal and vibration stability of the cavity.

3. **Mounting structure**: Back and forth between Step 3 and Step 2 is natural during the designing process. As discussed in the previous section, the mounting strategies are not universal and need to be tuned as per the geometry. This process is simulation-heavy and is the most time-consuming step. It is generally in this step that new techniques and/or structures are conceptualised and optimized.

4. **Materials**: Selection of the material of each and every component is vital. Optical, mechanical and thermal properties of the materials are closely considered in the process along with potential manufacturing challenges, and different combinations are virtually tested.

5. **Thermal shielding**: Thermal shielding is mandatory for both lab-based and transportable FP cavities. The structure is generally simple, but the components in contact are critical for performance. Active temperature control is optional.

6. **Integrating optics and electronics**: The cavity, along with the mounting and thermal shields, is enclosed in a vacuum chamber. This assembly is optically aligned with the laser, and integrated with the servo electronic hardware, resulting in a practically usable short-term reference laser system. The entire system is mounted on a commercially available 19" rack, ready for transportable applications.

2.2 Important definitions and symbols

Sl.no	Parameter	Description	Symbol	Remark
1.	Frequency noise	*Noise or spread in the resonance peak of the cavity frequency spectrum*	$\frac{\Delta\nu}{\nu}$	
2.	Relative Deformation	*Change in the cavity length, given by: (Deformation of the left mirror) - (Deformation of the right mirror)*	ΔL	Deformation of mirror surface along the cavity axis is considered.
3.	Relative length stability	*Change in cavity length normalised to the absolute length of the cavity*	$\Delta L/L$	
4.	Thermal stability	*The ability of the cavity to resist change in cavity length caused due to temperature fluctuations*	also denoted by $\Delta L/L$	
5.	Vibration stability*	*The relative length stability of the cavity experiencing 1g acceleration along the cavity axis*	$\frac{\Delta L}{L} \cdot g^{-1}$	
6.	Power Spectral Density (PSD)	*PSD describes the power distributed over frequency content of the random process (e.g., ground vibrations). It is computed by the Fourier transform of a time domain data stream.*	m^2/Hz	
7.	Allan variance (AVAR)	*Allan variance is used to assess the stability of a frequency standard over a time interval τ. AVAR is related to spectral density via:* $\sigma^2(\tau) = 2\int_0^\infty S(f)\frac{sin^4(\pi f\tau)}{(\pi f\tau)^2}df$	$\Delta\nu/\nu$ over integration time τs	Allan Deviation (ADEV) $(\sigma) = \sqrt{(AVAR)}$

** The definition of the vibration stability is inferred from the standard procedure performed to characterize the stability of the cavity against vibrations. Details in section 2.6.4.*

Table 2.1: Important definitions related to cavity stability and their symbols.

2.3 Sources of frequency noise

The frequency-to-length coupling between a laser and the cavity to which it is locked, provides the principle on which a cavity can generate a stable low-noise output. This implies, the length of the cavity, or more precisely the magnitude of relative length instability $\Delta L/L$ in the cavity, has to be kept under check.

The frequency output from a cavity-locked laser can inherit noise from multiple sources, that are broadly of two kinds: (i) noise sources of **optical and electronic** origin, which directly add frequency noise to the output spectrum; (ii) noise sources of **thermo-mechanical** origin, which affect the cavity length and thereby contribute to frequency noise.

Identifying each and every factor that can add to the noise, and making sure to adopt suitable measures to suppress or isolate different noises to the highest degree is an absolute challenge. In the following subsections, different noise sources are discussed in more detail.

2.3.1 Optical and electronic noise

- **Radiation pressure**: The instability caused due to the radiation pressure manifests in two ways. Primarily, the pressure distorts the mirror surfaces giving rise to change in cavity length. The other influence is imbibed into the calculation of the Brownian thermal noise in section 2.3.2. The former kind of instability due to radiation pressure, expressed in terms of relative length stability is given by [10]:

$$\frac{\Delta L}{L} = \sqrt{\frac{2(1-\sigma_{fs}^2)}{\pi^{3/2} c Y_{fs}} h\nu P_{circ}} \tag{2.1}$$

  where, σ_{fs}^2 and Y_{fs} are the Poisson's ratio and Young's modulus of the mirror substrate (fused silica), $P_{circ} = \frac{P_{in} t r}{(1-r)^2}$ is the power circulating inside the cavity (t and r are transmittivity and reflectivity of mirrors), h is Planck's constant, c is speed of light, and ν is the frequency of incoming light. Considering the typical input power of $1\mu W$ in cavities, and a finesse of 1×10^5, the order of instability due to radiation pressure is $\mathcal{O}(10^{-22})$. This value is much lower compared to the instability arising from other sources.

- **Electronic hardware noise**: The noise in electronic hardware comprises contributions from various components within the Pound–Drever–Hall locking system, including the source laser, actuator, servo, frequency discriminator, and photodetector. The noise is manifested in the form of Residual Amplitude Modulation

(RAM), which is the undesirable modulation in the system. To mitigate the frequency instability arising from RAM, an electro-optic modulator is employed in the PDH loop. This technique reduces RAM-induced frequency instability to approximately 75 parts per million (ppm) with respect to the cavity line-width, as demonstrated in previous studies [57].

Through experimental analysis conducted at the PQM Lab, IUCAA, the frequency instability of the PDH system due to RAM was determined to be $1.71(3)\times10^{-19}$. This assessment considered a commercially available laser, which exhibits an ADEV of approximately 1×10^{-10} over 1 s, along with digital servo electronics having an ADEV of approximately 3.3×10^{-18} over 1 s [10]. Importantly, the analysis highlights that the contribution of RAM to total cavity instability is negligible, being an order of magnitude smaller than other dominant instabilities.

- **Mode degeneracy**: Mode degeneracy is a kind of optical noise resulting from the overlapping of the Higher Order Modes (HOM) with the Fundamental Mode (FM) of the cavity, which can contribute to the frequency noise in the output. The HOMs present in a cavity depend on the radii of curvature of the mirrors, and the length of the cavity, which determines the resonant modes. The optical noise due to degeneracy of modes can be effectively suppressed by geometrical means. This is discussed in detail under Optical simulations, in section 2.6.2.

2.3.2 Thermo-mechanical noise

- **Pressure fluctuations**: The pressure variations inside the cavity bore can affect the local refractive index of the medium between the mirrors. As a consequence, the optical path length (nL) of the cavity and thereby resonance frequency experiences fluctuations. To minimize the impact of pressure fluctuations, the cavity is typically enclosed in a vacuum environment. For an ideal gas, fractional change in the refractive index $\frac{\Delta n}{n}$ induced by a change in pressure ΔP (in mbar) is associated to the gas particle polarisability a, as outlined by the relation [58]:

$$\frac{\Delta n}{n} = \frac{a}{2k_B T} \cdot 100 \cdot \Delta P \tag{2.2}$$

at temperature T (in K), and k_B being the Boltzmann's constant. For the gases common in vacuum (N_2, O_2, H_2O etc.), $a \equiv a_{vacuum} \approx 1.4 \times 10^{-30}$ m^3. A cavity enclosed in a vacuum chamber can therefore obtain a relative length stability below 10^{-16} by stabilising the pressure $\Delta P < 1.5\times10^{-9}$ mbar. This is a less strict requirement compared to cavity in air by five times [3].

- **Thermal noise**: The temperature fluctuations in any environment can cause expansion or contraction in the cavity spacer, mirrors, and mounting, causing fluctuations in the cavity length. This constitutes thermal noise, which is simply the frequency noise of thermal origin.

  Thermal noise is majorly tackled by right choice of constituent materials which have very low thermal expansion coefficients. Yet, a typical ceramic material, which is one of the best choices, used in cavity spacer has a minimum thermal expansion coefficient of $\mathcal{O}(10^{-9})$ m/K at optimum temperature. A simple scaling estimate reveals that for 1 mK rise in ambient temperature, the cavity length expansion can be a few picometers. Deformations of this order can definitely cause great instability. Hence, thermal noise is one of the dominant noise sources in causing cavity instability. The thermal analysis of the cavity involves designing proper thermal shielding to bring down the thermal fluctuations to a few μK, and also to identify the optimum temperature range for operating the transportable cavity.

- **Brownian noise limit**: The stability of the cavity's length is fundamentally limited by the Brownian motion of the particles in the constituent materials. Thermal fluctuations occurring within the mirrors and spacer introduce random variations in the optical path length, resulting in inevitable thermal noise. According to the fluctuation dissipation theorem [59], the spectrum of random motion, such as Brownian motion of the atoms within each component, correlates with the thermodynamic loss in the system. Hence, this relationship depends on material properties and the optical mode on the mirrors. The random displacement fluctuations induced by thermal noise is ultimately expressed in terms of power spectral density of frequency fluctuations. In depth analysis of the thermal noise limit derivation is beyond the scope of this thesis, but has been theoretically evaluated in [60–62]. Table 2.2 provides the Brownian noise calculated for cavities of different length and geometry.

Table 2.2: Estimated Brownian noise limit for transportable cavities with ULE spacer, fused silica mirrors and dielectric mirror coatings.

Cavity length (in mm)	Spacer geometry	Brownian noise floor (ADEV)
50.8	Spherical	$6.5\text{x}10^{-16}$ [41]
87	Cubic*	$3.7(6)\text{x}10^{-16}$ [53]
25	Cylindrical*	$1.6\text{x}10^{-15}$ [47]
100	Cylindrical	$4\text{x}10^{-16}$ [45]
200	Cylindrical*	$7\text{x}10^{-17}$ [49]
25	Tetrahedral*	$1\text{x}10^{-15}$ [50]

** Special ULE rings are used along with fused silica mirrors to reduce Brownian noise.*

In room-temperature cavities, the Brownian noise is contributed by each of the components including the spacer, mirror substrates, and mirror coatings. Contribution from each component vary based on their physical dimensions, mechanical loss factor, modulus of rigidity etc. For cavity with ULE spacer and FS mirrors, the Brownian noise of the dielectric mirror coatings is found to dominate over others (>70% in hemispherical cavities), despite the coatings being only a few micrometers in thickness. Cryogenic cavities and lower noise crystalline $Al_xGa_{1-x}As$ mirror coatings to replace dielectric mirror coatings are some of the recent advancements seen in reducing the effect of Brownian noise [63]. Table shows the Brownian noise limit estimated for some of the available room-temperature cavities.

- **Vibration noise**: The seismic activities are continuous and random processes giving rise to seismic vibrations. These vibrations are a major source of noise, as they travel from ground through the rack, and all the assembly components to reach the cavity mirrors. The mechanical vibration thus results in length fluctuations in the cavity leading to frequency noise. This is termed as vibration noise.

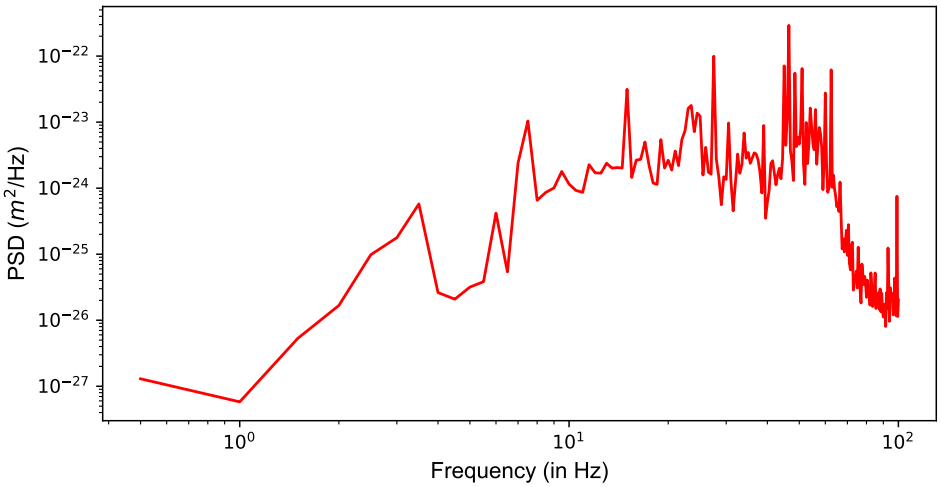

Figure 2.1: Deformation of the cavity mirror centre experiencing ground vibrations.

In a non-laboratory environment, the vibration levels are significantly higher compared to laboratory conditions. Fig.2.1 shows the frequency dependent deformations in a mirror experiencing seismic vibrations. The RMS deformation of the mirror, obtained by the area under the PSD curve, is 1.96×10^{-11}. This can cause significant change of cavity length if not addressed. In fact, mechanical vibrations are the most dominant form of noise source for transportable FP cavities.

From the above discussion, it can be concluded that the frequency noise arising from optical and electronic sources are significantly lesser in comparison to the noise arising

due to the length fluctuations in the cavity caused by temperature and vibrations. In conclusion, thermal noise and vibration noise are the two main dominating noises in a transportable cavity.

2.4 Materials used in transportable cavities

From the previous section 2.3, it is evident that the noises of thermal and mechanical origin have the maximum impact on the stability of the cavity. This is because they can directly influence the cavity length. Noises, thermal and vibration in particular, traverse from the environment to the system via the components – the shields, support structures, cavity-mounting contacts etc. and finally result in the deformation of the spacer and mirrors.

In the designing of a transportable cavity, several countermeasures are adopted to suppress or isolate the noises. One of the primary, and most effective measures is in being wary of the materials used throughout the cavity assembly. Selection of materials is a very critical phase in the designing process. The desired qualities in the material depends on the particular component and its function, but in general should resist thermal and vibration noise at its best. The materials should also be vacuum-compatible, and exhibit less ageing effects for durability.

In the years of research on transportable cavities, certain materials have repeatedly proven to produce the best results, and are commonly used in majority of the cavities. The rest of this section lists out different materials utilized in specific components, and their favourable thermo-mechanical properties.

- **Cavity spacer and mirror substrate**:
  The spacer and mirrors in a cavity need to sustain against both thermal and mechanical noises that effect cavity length. Ceramic materials offer high modulus of rigidity and low coefficients of thermal expansion (CTE). Ultra-low Expansion (ULE) glass, Zerodour, Sital and Sapphire are some materials that posses the favourable properties. Amongst these, ULE offers exceptionally low CTE and is widely used for spacers in Fabry-Pérot cavities. Fused silica (FS) substrates are nowadays more preferred for mirrors since FS not only has low CTE but also contributes very less Brownian noise. Additionally, both ULE and FS have high rigidity and low Poisson's ratio which adds to the mechanical stability of the cavity.

- **Mirror coating**:
  High reflectivity optical coatings are utilized for obtaining high finesse FP cavities. These coatings are made by deposition of alternating layers of high and low refractive index materials. Dielectric coating consisting of alternating layers of Ta_2O_5

and SiO_2 are popularly used in room-temperature cavities. However, these reflective coatings contribute significantly to the Brownian noise of the cavity.

- **Fixing patches**:
  The support patches act as the interface between the ULE spacer of the cavity and the metallic brackets. These patches not only facilitate the mounting of the cavity, but also need to provide good vibration stability. Following a previous design by NPL, UK [34], Room-Temperature-Vulcanising silicone (RTV silicone) is used for support patches in the cavity assembly.

- **Support/Mounting structures**:
  The mounting structure for transportable cavity needs to be strong and rigid to provide robust support for the cavity. Across different designs from the past, metallic supports of various forms and functions can be observed. Titanium (Ti) and Invar brackets are broadly used in many transportable cavity designs. Some have also utilized Aluminium and its alloys for better thermal properties.

- **Thermal shield**:
  Thermal shields assist in regulating the temperature fluctuations in cavity's environment. Using multiple layers (typically two to three layers) the ambient temperature fluctuations are brought down from mK to μK range. The contacts between the thermal shields are kept minimum to reduce thermal conduction. The major means of heat transfer is via radiation. Hence, the thermal shield material requires low emissivity along with low conductivity. Aluminium and alloys of aluminium are popular choice for thermal shields.

Table 2.3: Important mechanical and thermal properties of the materials used in transportable cavity designing. Ref.[10, 64]

	Density (kg/m^3)	Young's modulus (GPa)	Poisson's ratio	Bulk modulus (GPa)	Thermal conductivity (W/mK)	Emissivity
ULE	2210	67.7	0.17	34.2	0.745	1.31
Fused silica	2203	73.1	0.17	36.92	0.8	1.38
RTV silicone	1110	0.0017	0.48	0.014	1.2	-
Teflon	2175	0.575	0.46	2.40	0.3	-
PEEK	1300	3.6	0.38	5.00	0.55	-
Duralumin	2780	73	0.33	71.5	164	0.05

2.5 Challenges in designing a transportable Fabry–Pérot cavity

In section 2.3, all the sources of noise are considered and the order of the frequency noise contributed by each source are estimated. In order to obtain a stable low-noise frequency output, the transportable cavity has to be isolated from all the external sources of noise to the highest degree. The conclusion from the section 2.3 tells us that the thermo-mechanical noise dominates over all the other noises implying that the bottleneck for improved stability is in mitigating the noises of thermo-mechanical origin.

The current research efforts across the world are mainly focused on finding ways to subdue the thermal and vibration noise [51, 65–67]. These noises are random and vary from location to location. In a non-laboratory environment, one cannot control the external factors and the cavity has to be really robust. Compared to a lab-based cavity, the complexity of designing levels up for a transportable cavity owing to its additional requirements of being compact, held with stiff mounting, and power consumption limits. Addressing each type of noise can require one or several measures: choice of materials, geometry, or mounting technique making it an intricate multi-variable problem. The challenges in the approaches of dealing with each thermal and vibration noise are multi-fold and discussed further.

Controlling thermal noise:
Thermal noise occurs due to length fluctuations in the cavity components from the mismatch in thermal expansion (CTE) of the materials in response to the temperature fluctuation and the intrinsic Brownian noise of the materials. The former is generally tackled via two approaches: (i) use of ultra-low expansion (ULE) material to reduce the impact for thermal fluctuations, and (ii) enclosing the cavity inside multiple layers of thermal shields and a vacuum chamber to reduce thermal fluctuations itself.

ULE material is preferred for cavity spacer due to its extremely low thermal expansion coefficient. But for mirror substrates, the Brownian noise of the material dominates over the thermal expansion effects. Hence, fused silica substrates are used for mirrors, which has a slightly higher CTE, but a lower Brownian noise. However, this results in a mismatch between the CTEs of cavity spacer and mirror substrate leading to non-uniform deformations under thermal fluctuations. As for the Brownian noise, which is present at any temperature, the highest contribution comes from the mirror coatings. A common way used to mitigate this noise in lab-based cavities is to choose a longer cavity length, as the Brownian noise varies inversely with length [3]. However, longer cavities are not ideal for transportation because they account for higher vibration instability. Plus, they can violate SWaP requirements. Hence, one of the factors need to be compromised.

For transportable cavities, the thermal shields also need to be mounted rigidly. Rigid mounting can increase the contact surfaces, or, total contact area, which lead to increased thermal conduction. Conduction limits the thermal stabilization process in the cavity. Therefore, one has to come up with suitable mounts for the shields, while keeping the contact areas to bare minimum.

Controlling vibration noise:
The complexity in isolating the vibration noise persists due to the mounting requisites of the transportable cavity. In lab-based cavities, the mounts are just points at ideal locations (Airy points) over which the cavity is placed, without any compressive force or clamping. This is called "soft-mounting". Whereas, for transporting the cavity, it is required to make the mounting rigid as opposed to soft, in order to hold the cavity or fix it, so as to avoid disorientation, misalignment etc. This rigid mounting, during operation, couples the mechanical vibrations to the cavity more severely than a soft mounting would. Hence, the challenge is to design a mounting that is rugged enough for transportation, but is also "soft" enough to minimize the effect of vibrations during operation. Vibration noise being the most-dominant in non-laboratory conditions, transportable FP cavities are in general, **vibration-limited**. This makes the mounting technique the most crucial aspect of the design.

For certain geometries (e.g., spherical, cubical) the mounting requires compressive forces at different locations on the spacer to be rigidly held [41, 42]. Consequently, the forces applied on the spacer can deform the cavity. In order to minimize the effect of support forces, the mounting needs to be symmetric and the number of support points kept minimal. Even the area of support contacts is critical. In the best-case scenario, one has to find, through modelling and multiple iterations, a mounting arrangement that offers a zero-crossing behaviour in the deformation along the cavity axis.

Lastly, the vibration stability can be greatly improved through sophisticated and precise mounting structures, as shown by Webster & Gill [42], Argence et. al. [45] etc. In effect, a complex mounting design also increases the intricacies of machining, and manufacturing cost. Precise mounting also requires highly skilled manufacturing, assembling, and very low errors. Such facilities may not be feasible everywhere. Thus, while designing the mounting for the transportable resonator, the machining limitations and cost-effectiveness are also very practical factors that needs to be weighed in.

All the above challenges and noise sources need to be analysed, and the design of the transportable cavity assembly needs to be optimized according to the stability requirement before the machining process. This is done by performing meticulous simulations and quantitative analysis to understand the response of the cavity to various noises.

2.6 Modelling and quantitative analysis

The designing process of the transportable Fabry–Pérot cavity in this work broadly carries two objectives:

- Modeling: CAD Modelling of the cavity assembly (with mounting and shields) The modelling of the FP cavity and mounting structure is performed using the *SolidWorks* software. *SolidWorks* is a computer-aided design software used to create precise 3D models and drawings. It enables efficient designing of complex parts and assemblies for testing cavity and mounting designs, and is highly user-friendly. The parametric modeling capabilities in *SolidWorks* allow for easy modification and iteration of designs.
- Finite Element (FE) simulation: subjecting the model to the relevant load cases for "stability tests" to characterize the performance

This section mainly focuses on the different types of simulation analysis performed on the cavity. In the optical simulations, factors contributing to the frequency noise through the cavity optical modes are considered, and design conditions to suppress them are obtained. The thermo-mechanical analysis deals with the length fluctuations in the cavity due to various external effects, and is used to optimize the design features to enhance the stability. Each section on different type of analysis is structured to specify the objective, boundary conditions, and the assumptions or limitations of the analysis.

2.6.1 Finite Element Analysis

Finite Element Analysis (FEA) is a powerful numerical technique used to simulate and analyze complex systems and structures. It involves dividing a large system into smaller, interconnected elements, allowing for the approximation of continuous behaviors such as stress, strain, and deformation. By applying principles of physics, FEA enables one to predict how a structure will respond to various loading conditions and design changes. This predictive capability makes FEA invaluable in the process of designing a cavity. One can optimize designs, identify potential instabilities, and ensure the performance of the cavity before it is manufactured.

During the course of the thesis, the FE simulations are performed using ANSYS Mechanical. ANSYS Mechanical software is a finite element analysis tool used for physics and engineering simulation applications. It allows modelling of geometries and structures involved in designing of the cavity and has modules for different kinds of analysis.

FE simulations are broadly of two types:

1. Static analysis
2. Dynamic analysis

To characterize the vibration stability of the cavity, which is the main focus of this work, both kinds of analysis were utilized. The acceleration sensitivity analysis (static analysis) was performed using the Static Structural module of ANSYS. The Modal analysis and Random Vibration modules were used to test the stability under the frequency dependent time-varying vibrations. The methodology of the three kinds of analysis are elaborated in sections 2.6.3 & 2.6.4.

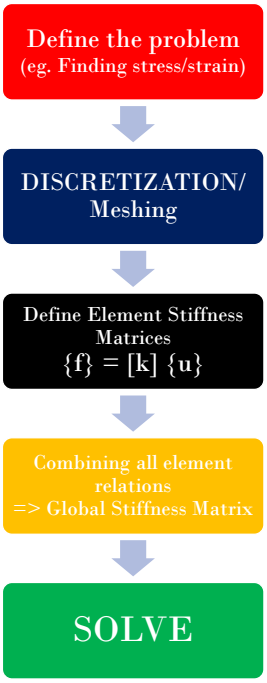

Figure 2.2: Schematic of the FE computation steps/procedures.

Meshing/discretization:

The dividing of a continuous body into a number of smaller interconnected elements is termed as discretization or meshing. Meshing is a very critical process that allows for the approximation of continuous variables like stresses and deformations in the body. Based on the shape and complexity of the body, ANSYS has automatic and customised assignment of different kinds of 1D, 2D or 3D mesh elements that are connected via nodes to accurately discretize the system. Some of the different mesh element types are represented in Fig.

The size of the mesh relative to the body size is another important aspect of the meshing. Naturally, the smaller the discrete mesh elements the better the approximation of the continuous variables. However, the discretization comes at the cost of computational burden. Finer meshing increases the number of nodes for computation and hence the computation time. In practice, the limit to finer meshing is often dictated by the RAM and processor speed. In order to find the optimum mesh size that is good enough for approximation as well as provides results within reasonable time, mesh sensitivity analysis is always paired with different types of FEA simulations. Mesh sensitivity analysis is simply the tracking of the continuous parameter with changing mesh size. Mesh sensitivity curves are plotted for bodies to determine the plateau region of the curve which indicates consistency in the value of the approximated variable against change in mesh size. At this mesh size value the parameter is said to have stabilised.

(a) Tetrahedral 3D mesh elements in cavity spacer and hexagonal mesh elements for mirrors & patches.

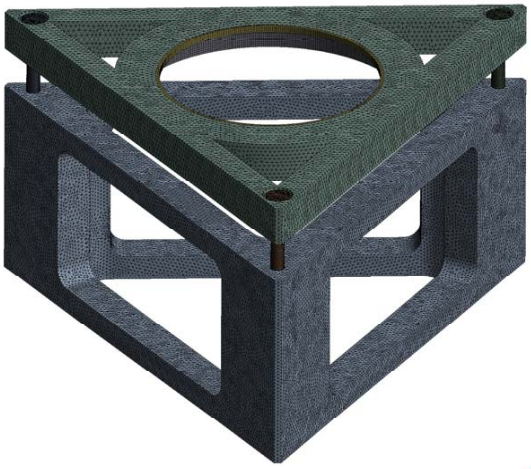

(b) Tetrahedral element meshing for brackets and screws of the mounting structure.

Figure 2.3: Different mesh element types used in ANSYS depending on the complexity of the structure. The geometry of the cavity spacer and designing of the mounting structure is explained in sections 3.2 and 3.3.

2.6.2 Optical simulations

The optical modes of the cavity can contribute to the frequency noise due to Higher Order Mode (HOM) degeneracies. HOM degeneracy means that the higher order transverse modes of the cavity are co-resonant with the fundamental mode. To effectively minimize this noise, one not only has to check for the co-resonant HOMs, but also suppress the optical powers distributed to the higher-order modes to avoid their mutual over-lapping.

The fundamental modes and HOMs depend on the cavity mirror configurations, and the precise length of the cavity. For reference optical resonators a commonly used mirror configuration is the hemispherical cavity, with $R_1 = 1$ m and $R_2 = +\infty$. The mirrors of specified ROCs are commercially available, and have good tolerance. The issue of frequency noise due to the HOM coupling can be resolved by finely tuning the length of the cavity, which suppresses the power of the HOMs. This technique is called the length optimization, adopted from the Ref.[3, 10].

Length optimization

The transverse optical modes in a cavity are described by Hermite-Gaussian (HG_{nm}) polynomials, where m and n are HG indices, with $m = n = 0$ corresponding to the cavity

Fundamental Mode (FM). To reduce the degeneracy of HOMs within a cavity, cavity length L must be selected carefully to ensure that the HOMs are not only resonant with the FM but also have power levels significantly lower than the detector's noise floor.

In order to check for co-resonant modes, the transverse mode separation frequency which is the frequency separation between two consecutive modes is calculated using [3]:

$$\Delta\nu \equiv \frac{\zeta}{2\pi}\Delta\nu_{FSR} \tag{2.3}$$

$$= \frac{1}{\pi}\cos^{-1}\left[\pm\sqrt{\left(1-\frac{L}{R_1}\right)\left(1-\frac{L}{R_2}\right)}\right]\Delta\nu_{FSR} \tag{2.4}$$

where, $\zeta = 2\cos^{-1}(\pm\sqrt{\mathcal{G}_1\mathcal{G}_2})$ is termed as the Gouy phase shift. Further, to estimate the power distributed across the higher order modes the suppression quality of HOMs normalised to the power of FM is given by [68]:

$$\kappa_{nm} \equiv \left[1+\left(\frac{2\mathcal{F}}{\pi}\right)^2\sin^2(n+m)\frac{\zeta}{2}\right]^{-\frac{1}{2}} \tag{2.5}$$

where, κ_{nm} is called the suppression factor, and $\mathbf{F}$ is the finesse of the cavity.

While optimizing the length of the cavity, a fixed number of higher order modes are considered, and using eq.2.3 and 2.5 the closest separation between the FM and the HOM is determined, while the sum of the powers of all the HOMs considered is evaluated. The optimum length is where the the closest HOM is sufficiently separated and also the sum of the powers of the HOMs normalised to FM is significantly suppressed.

2.6.3 Vibration analysis

- **Objective**:
  The mechanical vibrations in the external environment, or generated within the system can couple to the resonator and cause length fluctuations. Random vibrations can exist across any frequency range. Transportable cavities are most susceptible to vibrations in the low frequency range, particularly from 1-100 Hz. Out of the many sources of vibrations, a prominent one is the seismic vibrations emerging from the ground, which fairly lies in the frequency range of interest. Hence, one desires to know the effect of these vibrations on the cavity deformations.

- **Procedure/boundary conditions**:
  The nature of seismic vibrations is random. Therefore, we cannot assess the stability of the cavity by merely coupling the seismic vibrations to the cavity. The standard procedure implemented towards characterising the vibration stability of the transportable cavity is by analysing its acceleration sensitivity. The cavity assembly is subjected to an acceleration of constant magnitude uniformly over the entire body, and the deformations in the cavity mirrors are analysed. The relative length change thereby obtained can be re-scaled to the magnitude of the ground vibrations in its power spectral density using appropriate methods. The acceleration sensitivity before the scaling is quoted in $\frac{\Delta L}{L} \cdot g^{-1}$ units.

- **Assumptions and limitations**:
  The supports and connections are very critical in vibration analysis. For the ease of modelling and simulations, structures are sometimes simplified, and the contacts are assumed to be ideal (bonded contacts). In reality, the contacts, especially the connections via the screws, are more complex and depend on the bolt pre-loads, which is not included in the modelling. The acceleration sensitivity analysis described above is only a standardised procedure to compare the stability, but does not entirely represent the vibration sensitivity due to the absence of any frequency dependence. Hence, this analysis is always combined with Random vibration analysis. During the vibration analysis, only the essential structures, i.e., spacer + mounting, is considered in order to effectively reduce the computational time. Due to the limitations of computational power, one may not be able to perform the vibration analysis on the entirety of the transportable resonator assembly.

2.6.4 Modal analysis and random vibrations

- **Objective**:
  Mechanical vibrations are frequency dependent. The true response of the cavity coupled to random vibrations is also frequency dependent. This means, the deformations suffered by the cavity depend not only on the magnitude of the vibrations, but also its frequency. The different components of the cavity can also exhibit resonance behaviour in deformations. Therefore, knowing the natural modes of vibration of the cavity assembly is extremely essential. This is performed through Modal and Random vibration analysis.

- **Procedure/boundary conditions**:
  The modal analysis module of the ANSYS software has an in-built feature to extract the natural resonant modes of any given structure, and also generate modal shape

results. The cavity spacer generally has very high natural modes ($>$ 1kHz). A rule of thumb is to design the mounting in such a way that the resonant modes of the cavity assembly is quite above the low frequency range (0-100Hz). If the condition is not met, the modal shape results help us identify the weakest structure in the mounting. This is then modified accordingly to increase the natural frequencies of the system. The second phase is the Random vibration analysis. The seismic vibrations are coupled to the cavity assembly through input PSD, and the deformations due to vibrations are studied. The software utilizes the modal analysis results, and includes the effect of natural modes while estimating the deformations.

- **Assumptions and limitations**:
  Random vibrations are stochastic. The deformations obtained from the analysis are not absolute but standard deviation values. The RMS magnitude of the deformations is calculated from the response PSDs, but the direction of deformation in individual mirrors is lost. Due to this, the relative deformation or the change in cavity length cannot be determined, since one has no way of knowing whether the individual deformations are in-phase or out of phase. The random vibration analysis can estimate the RMS deformations in the cavity. But in long term, the effect of ageing becomes relevant since vibrations act as continuous loads on the cavity. The cavity can only be used as short-term reference, because its stability can vary in long timescales. This is the reason why FP cavities are called "fly-wheel oscillators". In the current simulations, it is not trivial to include such long-term effects during the analysis.

Chapter 3

Results and discussion

In this chapter, all the analytical and simulation results obtained at different stages of designing the transportable FP resonator are presented. The conclusion from each section helps us in determining a certain structural feature of the design. The majority of the factors influencing the design of the cavity presented here emerge from the stability analysis under vibration. The completeness of the designing process is subject to the thermal stability analysis, largely, and further assembling of vacuum chamber, optics module, and electronics rack which is not a part of this thesis.

3.1 Length optimization

As outlined in the overview 2.1, the designing process begins with the selection of the length for the cavity. A smaller length is desirable in transportable cavities, since it makes the system compact and lightweight. In some of the previous attempts [47, 50], the cavities were made ultra-compact by choosing a very small length of <50 mm. These cavities do not provide high frequency stability due to the Brownian noise limit in smaller cavities 1.11. Taking this into consideration, a reasonable length-scale for the cavity close to 100mm is chosen for better performance against Brownian noise. Subsequently, to optimize the cavity length, a length-scan is performed close to 100 mm to find the precise length at which the power from the higher order modes is maximally suppressed.

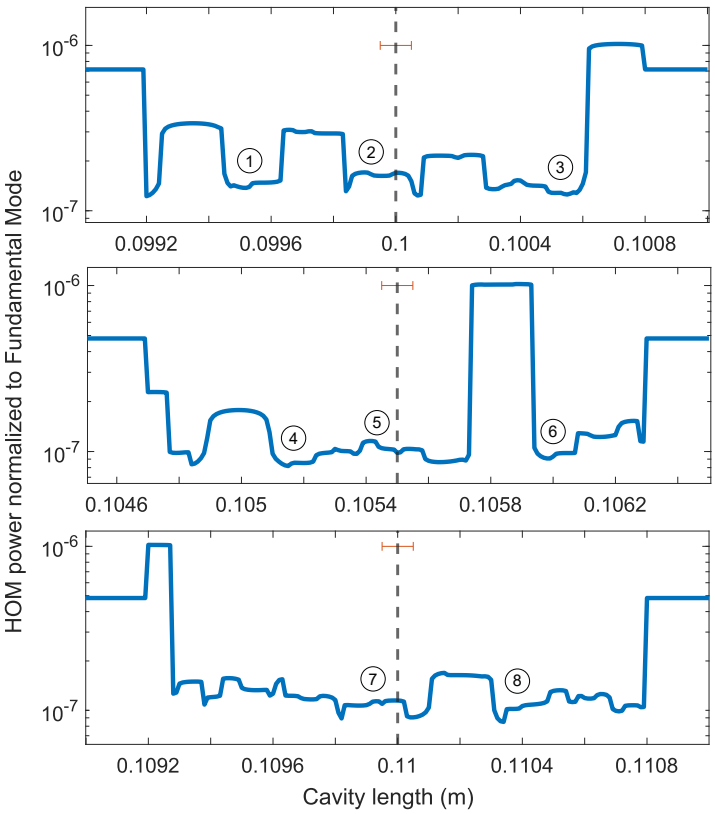

Figure 3.1: Normalised power of first 200 Hermite-Gaussian modes for varying cavity lengths. The error bar corresponds to a tolerance in length of $\pm 100 \mu m$.

Region	HOM power
1	1.38×10^{-7}
2	1.62×10^{-7}
3	1.25×10^{-7}
4	9.76×10^{-8}
5	9.92×10^{-8}
6	9.78×10^{-8}
7	1.14×10^{-7}
8	1.05×10^{-7}

Figure 3.2: The averaged suppressed HOM power (considering tolerance of $\pm 100 \mu m$) at different plateau regions of the normalised power curve corresponding to different cavity lengths.

Fig.3.1 shows the distribution of power in HOMs normalised to the power of the fundamental mode for different cavity lengths. The ROCs of the cavity mirrors are $R_1 = 0.5$ m & $R_2 = +\infty$. The Hermite-Gaussian modes up to $n + m = 200$, where m & n are mode indices, within ± 10 MHz of the fundamental mode are considered. The distribution shows multiple minima across different ranges of length. But one also needs to consider

the fact that matching the exact length can be practically challenging. Hence, flat minima are more favourable compared to sudden dips, since they offer better suppression of HOMs within the tolerance limit. Three valleys were found with very close maximally suppressed power values, and one of them is arbitrarily chosen.

The chosen cavity length in this case is **105.5 mm**, which corresponds to an FSR of 1.42 GHz. At this length, it is found that the closest HOM is 252 kHz apart from the fundamental mode, which is about 25 times the line-width of the cavity frequency spectrum (for an estimated finesse of $\mathcal{F} = 10^5$).

3.1.1 Associated Brownian noise:

The Brownian noise expressed in terms of frequency dependent thermal displacement fluctuations, can be appropriated to the fractional frequency noise in the cavity using the formalism described in [3]. For the given cavity length of $L = 105.5$ mm, with ULE glass spacer, fused silica mirror substrates and dielectric mirror coating, the spectral frequency noise is plotted for an input power of 1 μW at λ =1550 nm. The material properties considered for the calculation are mentioned in section 2.4.

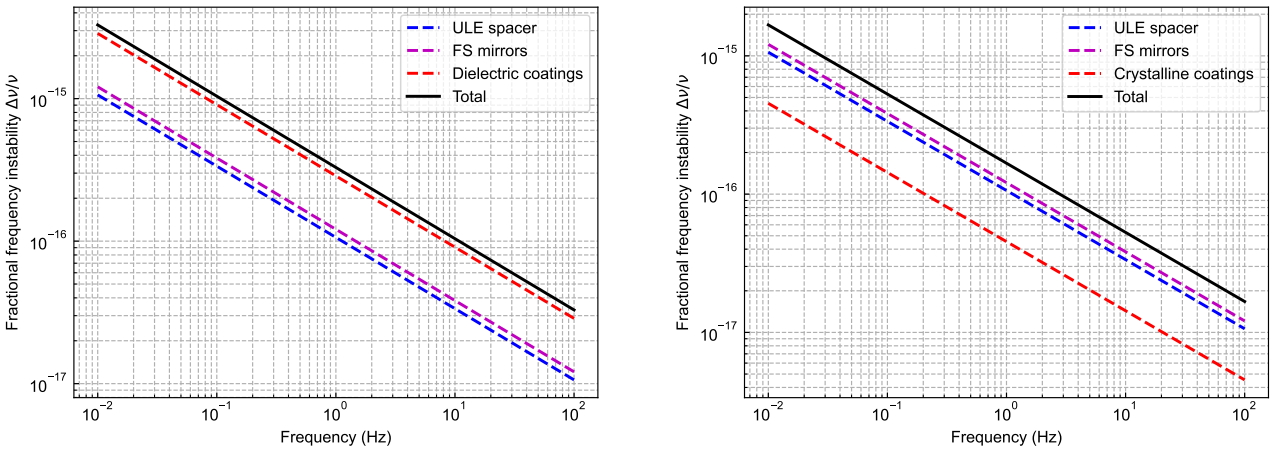

(a) (b)

Figure 3.3: Fractional frequency instability due to Brownian noise for a cylindrical cavity cavity of length L =105.5 mm with (a) dielectric coatings and (b) crystalline coatings, at T =300 K with radius of curvatures of the mirrors $R_1 = 0.5$ m and $R_2 = +\infty$.

The geometry of the spacer does not play a major role, since the dominant contribution is from the dielectric mirror coatings (Fig.3.3a). With use of crystalline mirror coatings the Brownian noise limit can be reduced as shown in Fig.3.3b, but requires cryogenic temperatures. At a constant temperature of $T = 300$ K, the estimated Brownian noise for the cavity in terms of fractional frequency noise is $\mathbf{3.3{\times}10^{-16}}$ at 1Hz.

3.2 Geometry selection

The geometries utilized for the spacer amongst the available transportable cavities include sphere [41], cube [42], cuboid [39], cylinder [45, 54] etc. These simple geometries are adopted based on their symmetry and effective mounting strategies. In theory, there is a myriad of spacer geometries and mounting structure combinations that one can conceptualize. However, an arbitrary geometry or an intricate mounting scheme can be challenging to manufacture and assemble, and therefore not very practical. Generally, the spacer geometries are either rudimentary or obtained through simple modifications of the standard geometries. One ought to wisely choose the geometry for the spacer based on compactness, stability demands, Size, Weight, and Power (SWaP) limitations, and feasibility of machining.

The cavity size (or volume) V scales with the cavity length L:

$$V \propto L^n \cdot a^p \cdot b^q \qquad \text{where,} \quad n+p+q=3 \tag{3.1}$$

The indices n, p and q are dependent on the spacer geometry, a and b are dimensions in other two directions. Therefore, the geometry is not only critical for innovating mounting techniques but also in maintaining the compactness. For example, in spherical and cubical geometries ($n = 3$), the volume scales quite rapidly with increase in cavity length. Whereas, in cylindrical or cuboidal geometries ($n = 1$), the scaling is only along one-dimension. From the basic cylindrical geometry, the volume can be reduced even further, by considering a "tapered-cylinder" geometry, Fig.3.4. A tapered cylinder is obtained from a regular cylinder by removing mass along a slope, from both the ends of a cylinder till its mid-plane. This geometry removes the additional mass from a cylinder to make the cavity smaller and lighter. For a given cavity length, a tapered cylinder offers one of the smallest spacer volumes. This factor makes the tapered cylinder geometry a potential candidate for transportable cavity.

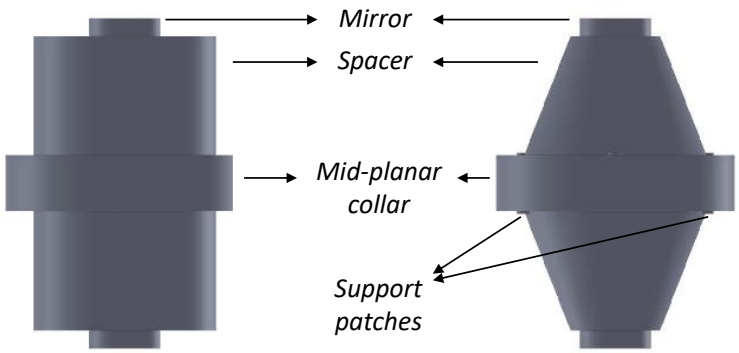

Figure 3.4: Cylinder and tapered cylinder spacers of similar dimensions with collars.

Table 3.1: Comparison of size and mass of different spacer geometries for increasing cavity lengths.

Geometry	l = 100 mm		l = 150 mm		l = 200 mm	
	Volume (in L)	Mass (in kg)	Volume (in L)	Mass (in kg)	Volume (in L)	Mass (in kg)
Sphere	0.52	1.14	1.75	3.88	4.17	9.22
Cube	0.98	2.16	3.34	7.38	7.95	17.57
Cylinder	0.36	0.80	0.52	1.14	0.67	1.49
Tapered cylinder	0.25	0.55	0.34	0.76	0.43	0.96

**The cylinder and tapered cylinder geometries are considered along with mid-plane collars. The radius for the cylinder and major radius for the tapered cylinder are both 32.67mm. The mass is calculated considering the density of ULE material.*

Mid-plane collar: A similar geometry has been used for transportable cavities previously by NPL, UK [44], and JPL, NASA [56]. The spacer has a mid-plane collar, which is an essential component of the design as it acts as an appendage for fixing the spacer with its mounting structure. The mounting forces can be decoupled more effectively when applied on the collar, rather directly on the spacer body.

Mounting orientation: The tapered cylinder cavity can be mounted horizontally or vertically using the collar structure. Considering the symmetry of the geometry along the cavity axis, the vertical mounting is deemed more suitable compared to a horizontal mounting. The static deformation of the mirrors due to self-weight is analytically found to be uniform for vertical mounting.

Mounting interface: The cavity spacer will be fixated to its designated mounting frame via the mid-planar collar. For this purpose, we consider a symmetric six-point mounting to provide sufficient support while keeping the support contact area to minimum. The support interface are patches made out of RTV silicone, affixed to the lower and upper surfaces of the collar (three patches on top and three below), at an angular separation of 120 degrees between them.

The dimensions of various design parameters of the tapered cylinder cavity are listed in the tables 3.2 and 3.3 below.

Table 3.2: Spacer dimensions

Parameter	Value (in mm)
Length (L)	105.5
Bore radius (b)	5
Minor radius (r)	16
Major radius (R)*	32.67
Collar radius (c)	42.67
Collar thickness (t_c)*	20

* Post optimization. Ref. 3.2.1.

Table 3.3: Mirror dimensions

Parameter	Value (in mm)
Diameter (D)	25.4
Thickness (t_m)	6.35

Table 3.4: Support patch dimensions

Parameter	Value (in mm)
Diameter (d)	5.00
Thickness (t_c)	1.00
Support radius (s)	37.67

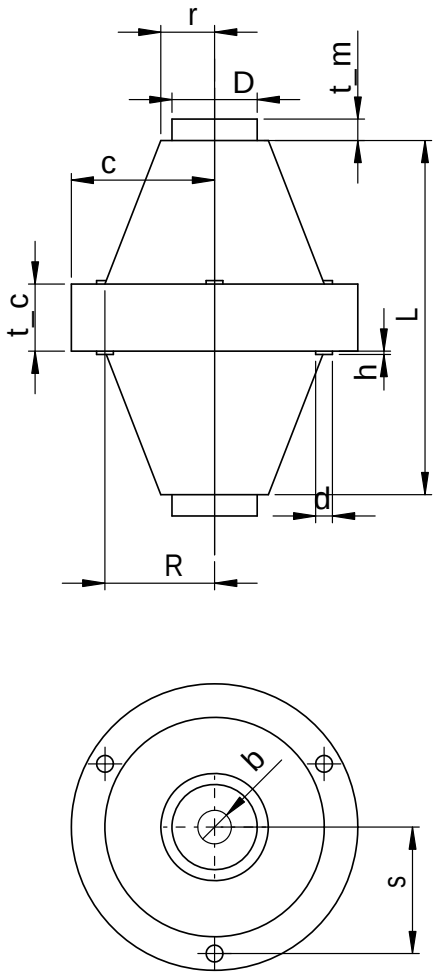

Figure 3.5: 2D sketch of the tapered cylinder cavity.

3.2.1 Stability comparison with cylindrical cavity

Zero-crossing in cavity deformation:

The mounting forces experienced by the cavity spacer through the support contacts can significantly influence the deformations of the cavity. To counter this, some of the spacer geometries showcase a favourable behaviour when a specific design parameter is optimized. In the spherical cavity developed by Leibrandt et. al [41], a mounting technique was demonstrated where the compressive forces of the two-point mounting is applied at a certain angle with respect to the cavity axis. At this "magic angle" the mounting forces effectively cancel out to give near zero-deformation along the cavity axis. This behaviour is known as the "zero-crossing in cavity deformation". This behaviour is one of the best ways to characterise the vibration stability of the cavity. Such techniques have also been shown for cubic [42], and cylindrical cavities [47].

The mounting scheme opted for the cavity involves supporting the cavity on the lower surface of the mid-plane collar via three symmetrically located patches. For this mounting, zero-crossing in deformation for acceleration sensitivity analysis was demonstrated in tapered cylinder geometry by NPL, UK [44], by fixing the minor radius and scanning the major radius of the cavity. The zero-crossing is also observed for regular cylindrical geometry, with vertical mounting, and a similar mounting scheme, via radius optimization. For tapered cylinder geometry there are multiple ways to achieve the said zero-crossing. By exploring the phase space of different parameters of the cavity and observing zero-crossing, we deduce two important results:

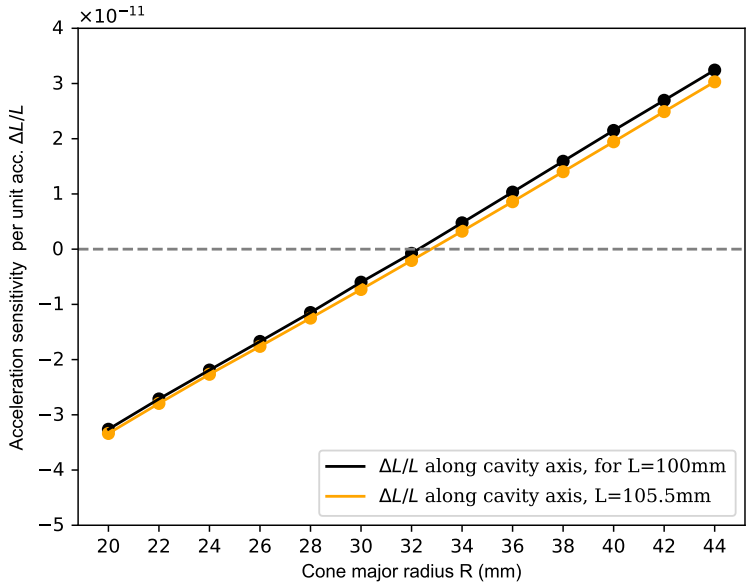

Figure 3.6: Zero-crossing in deformation for tapered cylinder geometry obtained for cavity length L=100 mm in [44], and for L=105.5 mm in this thesis.

1. Comparing the stability between cylindrical and tapered cylinder cavity
2. Optimising the parameters of the tapered cylinder geometry

The results of the parameter scan and the observed zero-crossing are discussed below.

I. Zero-crossing in symmetric and asymmetric spacers:

Fig.3.6 shows the primary result where the zero-crossing is obtained for a 105.5 mm cavity with minor radius $r = 16$ mm and collar thickness $t_c = 20$ mm. Two relations are defined amongst the parameters: $s = R + 5$ mm for support patch radius and $c = R + 10$ mm for collar radius. For smaller values of the major radius, the relative length change is negative, implying that the cavity is contracting. At larger major radii, the cavity starts expanding. The zero-crossing is achieved in between at $R = 32.67$ mm for the above specified spacer dimensions and constraints. This provides the first candidate spacer configuration for the cavity, with finalised dimensions as mentioned in table 3.2.

For a cylindrical spacer, since $r = R$, major and minor radii evolve together. For a cylindrical spacer defined under similar constraints, the zero-crossing is obtained for $r = R \approx 39$ mm (Fig.3.7). This configuration, even though achieves zero-crossing, is simply of larger volume. Hence, is not preferred over the tapered cylinder geometry.

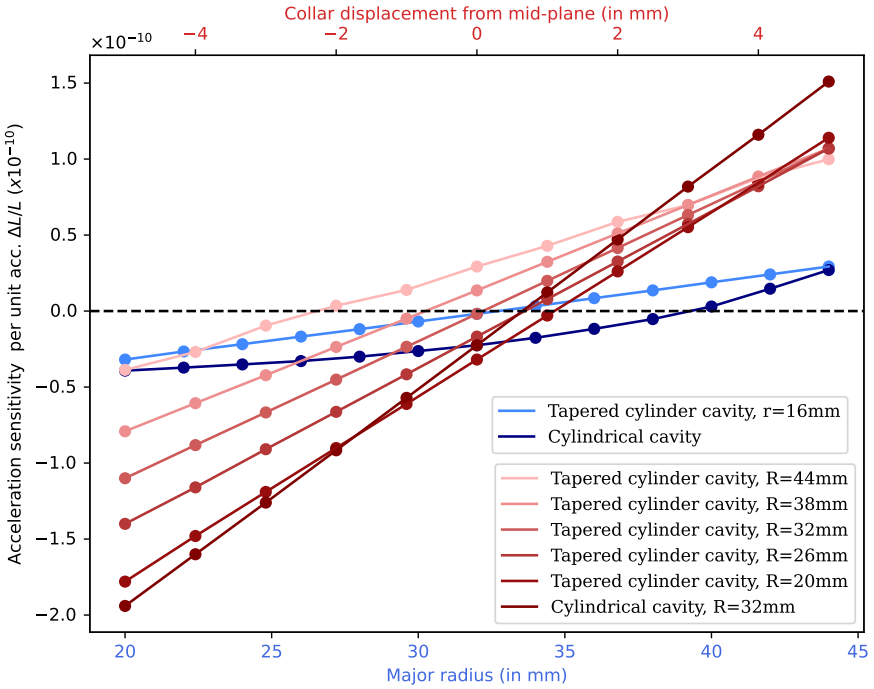

Figure 3.7: Comparison of zero-crossing curves for acceleration sensitivity analysis between cylindrical and tapered cylinder geometries, for 1 m/s^2 along cavity axis.

Table 3.5: The slopes of the zero-crossing curves for asymmetric cavities. The symmetric cavity with major radius = 32.67 mm has the least slope, hence best tolerance.

Major radius at zero-crossing (in mm)	Slope of the zero-crossing curve (a.u.)
20	2.91×10^{-11}
26	2.47×10^{-11}
32	2.16×10^{-11}
38	1.86×10^{-11}
44	1.39×10^{-11}
32.67 (Symmetric cavity)	$\mathbf{2.54\times10^{-12}}$

An alternate approach to achieve zero-crossing is to vary the position of the collar away from the mid-plane, while all the remaining parameters including the major radius, are kept constant. Fig.3.7 shows that appropriate displacement of the collar can result in zero-crossing of the tapered cylinder cavity for major radius other than 32.67 mm too. But as a consequence, the cavity becomes asymmetric. The slopes of the asymmetric cavities being higher than the symmetric cavity indicates that the stability is more sensitive to tolerance in machining. The cylindrical geometry with 32 mm radius also suffers from high sensitivity compared to the tapered cylinder geometry with the same major radius. Therefore, it does not provide any advantage in choosing any of these cavity configurations.

II. Varying major radius for different minor radii values:

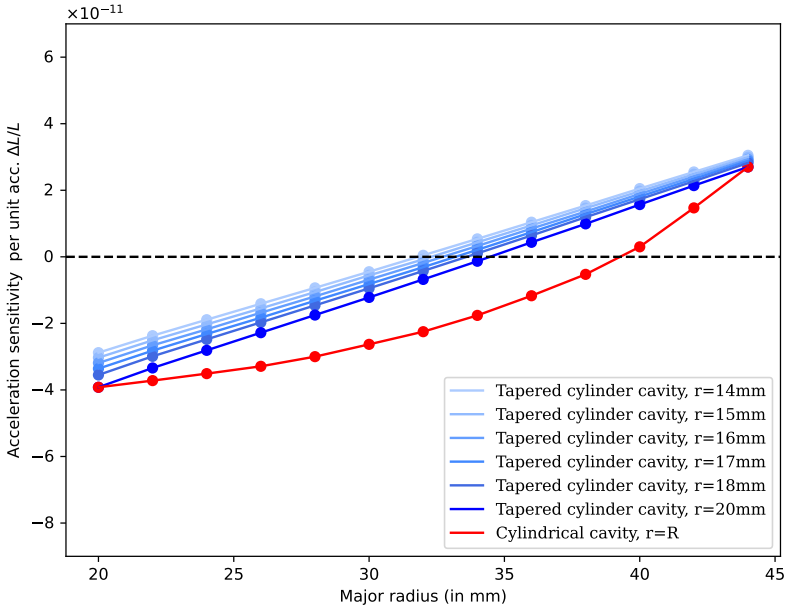

Figure 3.8: Comparison of zero-crossing curves for acceleration sensitivity analysis of tapered cylinder spacer with different minor radius values, at 1 m/s^2 along cavity axis.

The dependence of the zero-crossing major radius for the tapered cylinder on the values of spacer minor radius is also checked. It is observed that the minor radius has very little effect. For different values of minor radius the acceleration sensitivity curve only shifts along the x-axis, changing the major radius values by a small amount. The minor radius cannot be reduced beyond a limit, since the spacer ends need to offer sufficient surface area for the cavity mirrors. For convenience, we stick to $r = 16$ mm, providing enough area for fixing the mirrors. The acceleration sensitivity curve for the cylindrical spacer can also be compared with the tapered cylinder configurations (Fig.3.8).

III. Varying major radius for different collar thickness:

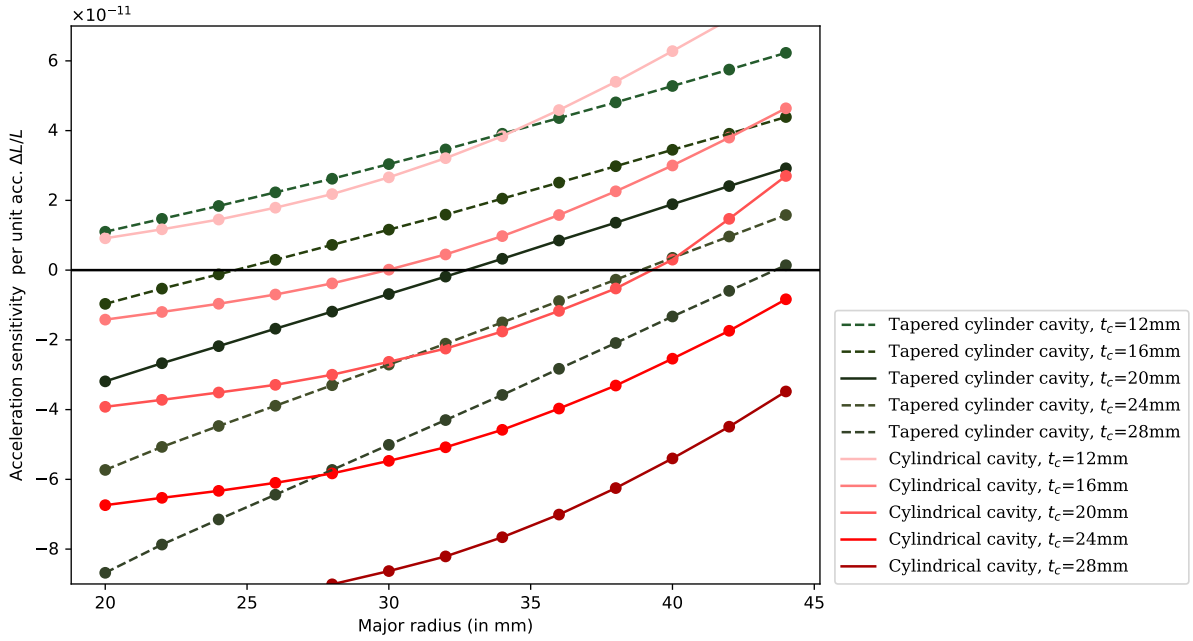

Figure 3.9: Comparison of zero-crossing curves for of tapered cylinder and regular cylinder spacers with different collar thickness, at 1 m/s^2 along cavity axis.

Table 3.6: The slopes of the zero-crossing curves for symmetric cylinder and tapered cylinder cavities with different collar thickness.

Collar thickness of considered symmetric cavities (in mm)	Slope of the zero-crossing curve for cylinder and tapered cylinder respectively (a.u.)
12	3.02×10^{-12} ; 2.14×10^{-12}
16	2.50×10^{-12} ; 2.23×10^{-12}
20	2.57×10^{-12} ; 2.54×10^{-12}
24	2.40×10^{-12} ; 3.03×10^{-12}
28	2.62×10^{-12} ; 3.65×10^{-12}

Lastly, the zero-crossing major radius is found to be influenced by the thickness of the spacer collar. The position of the collars are maintained in the mid-plane, but collars of different thickness are considered for stability analysis. For both tapered cylinder and regular cylinder, the value of major radius at which zero-crossing is achieved increases with increasing collar thickness t_c. The geometries attaining near zero instability for larger major radius and collar thickness are not interesting due to their larger volume and mass. However, we find two other configurations which achieve zero-crossing as well as have volumes similar or smaller than the tapered cylinder spacer considered earlier. These favourable features make the spacers worthy of consideration.

The analysis of zero-crossing in cavity deformation for the pre-determined three-point symmetric mounting scheme provides us with three spacer candidates with optimized parameters as listed in the table 3.7 below:

Table 3.7: Optimised spacer geometries obtained through acceleration sensitivity analysis.

Geometry	Optimized parameters (in mm)	Volume (in L)
Tapered cylinder (I)	$R = 32.67$, $r = 16$, $t_c = 20$	0.38
Tapered cylinder (II)	$R = 24.50$, $r = 16$, $t_c = 16$	0.27
Regular cylinder	$R = 30.23$, $r = 16$, $t_c = 16$	0.17

3.3 Mounting structure and design

Lower bracket

For the 3-point symmetric mounting of the cavity spacer, a pyramidal bracket structure was designed on which the spacer is mounted. The lower surface of the cavity mid-planar collar is fixed to the upper horizontal beams in the bracket, using the three support patches made of RTV silicone. The bracket is monolithic, and made entirely out of metal. The mounting in our case is on a single rigid structure, as opposed to the independent Teflon rods or titanium legs used in some previous attempts for a similar geometry and orientation [46].

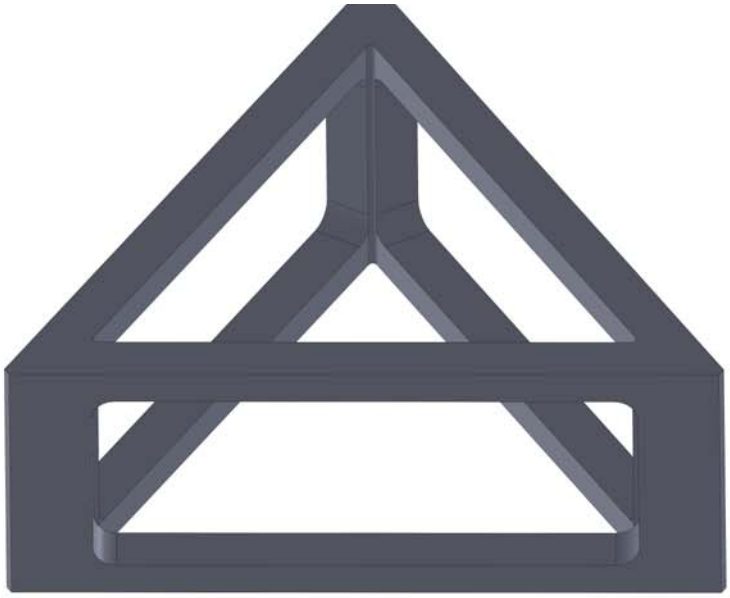

Figure 3.10: Monolithic lower bracket for cavity mounting.

The thickness of the beams and legs are adjusted to offer sufficient mounting area for the spacer, and also strengthen the bracket. The additional mass removed from the monolithic metal block to create the bracket frame, reduces the excess mass of the mounting structure. Overall, the design keeps the bracket light, but also rigid enough for transportable cavity.

The design of the bracket was intuitively developed. The stability of the mounting is subject to vibration and modal analysis. (The exact dimensions of the bracket can be obtained from the author on request.)

Upper bracket:

The lower bracket is used to firmly fix the cavity in a vertical orientation. This constrains the cavity motion along the vertical direction. In order to constrain the cavity motion in the remaining two directions, a triangular bracket is used from the top of the spacer. The upper bracket is obtained by hollowing certain regions of a thick triangular metallic plate, in such a manner that, the cavity collar firmly fits inside the hollow region of the frame. The top frame is essentially attached to the upper surface of the cavity collar, via three RTV silicone support patches, in a way similar to the cavity mounting on the lower bracket. But an additional contact is established between the cavity and upper bracket by using "fillers", of a suitable material, between the hollow inner surface of the frame and the curved surface of the collar.

Three different variants for the upper bracket were considered:

Sl. no.	Bracket type	Mass* (in kg)
1.	**Solid plate**	0.16
2.	**Semi-hollow**	0.12
3.	**Thin plate + ring**	0.05

** for Duralumin material*

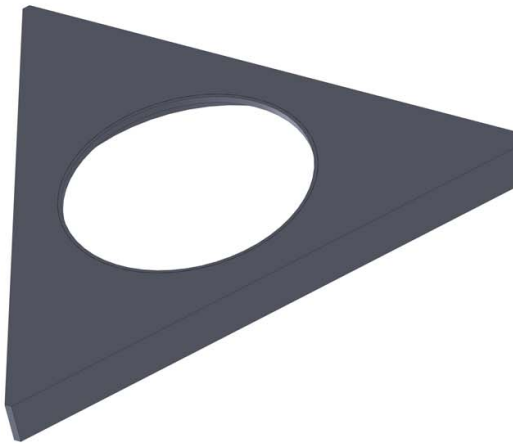

Figure 3.11: Variant-I: Solid bracket

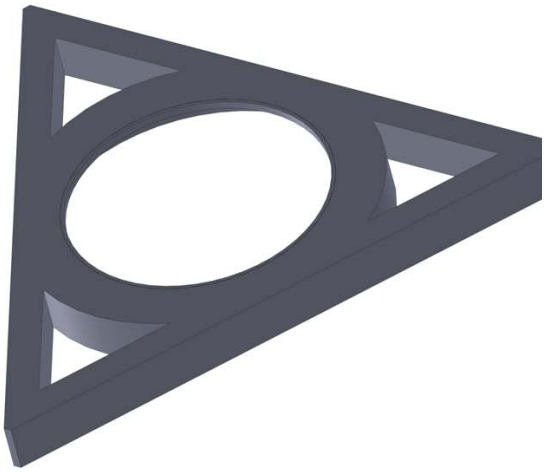

Figure 3.12: Variant-II: Semi-hollow

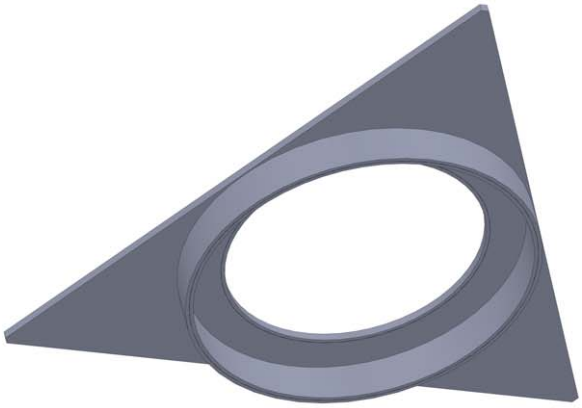

Figure 3.13: Variant-III: Thin plate bracket

Finally, the top frame is rigidly held by fixing it to the lower bracket using three identical screws. This completes the mounting of the cavity spacer, and effectively constrains the cavity motion in all the three directions. There is no use of any compressive force for mounting, except for the initial sagging due to the tightening of the screws and self-weight of the system.

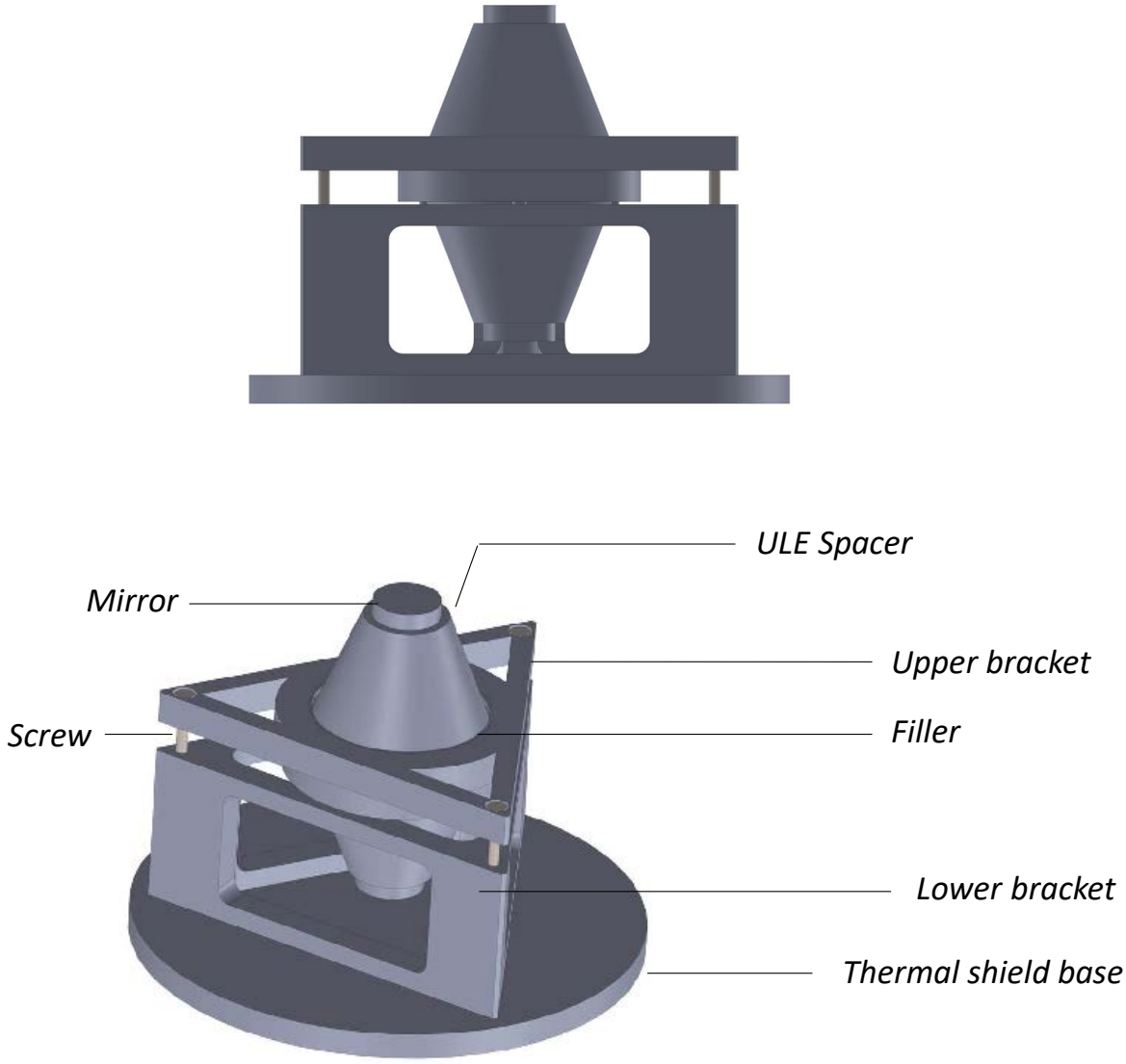

Figure 3.14: The entire cavity assembly with the spacer mounted on the upper and lower brackets, and held by three identical screws. The assembly will be fixed to the base of the inner-most thermal shield layer.

The vibration stability and modal frequencies for the three models are analysed. Different materials for the filler (RTV silicone, Teflon, PEEK) and metal brackets (Duralumin, Invar, Titanium) are tested. The screw size is also a variable parameter in the model and is suitably optimized.

3.4 Vibration analysis

3.4.1 Mesh sensitivity analysis

The mesh sensitivity analysis was performed for the full cavity-mounting assembly in order to find the suitable mesh size for the analysis. Generally, a uniform mesh size is chosen for all the components. But as the model becomes more complex, the simulation may take very large computational time, or just fail due to insufficient memory to store intermediate results. Hence, the mesh size was optimized individually for every component.

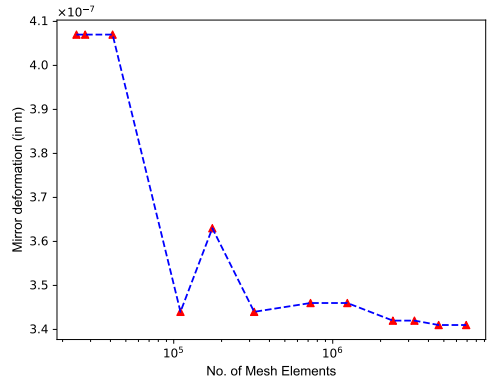

(a) Mesh sensitivity for cavity spacer

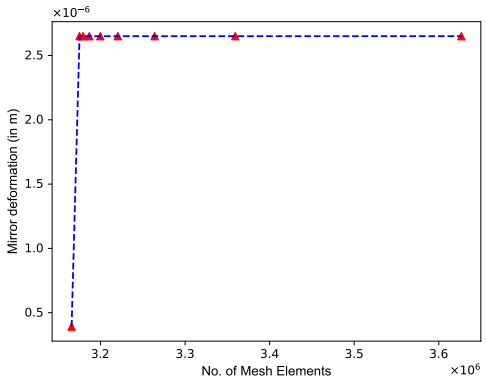

(b) Mesh sensitivity for cavity mirror

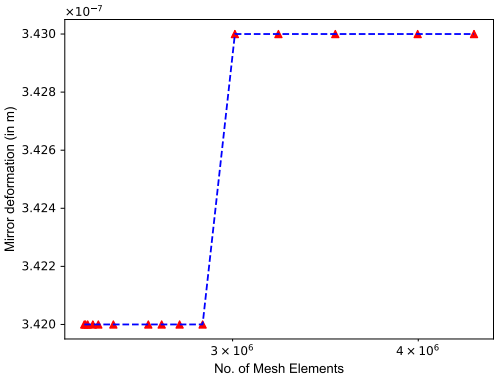

(c) Mesh sensitivity for lower bracket

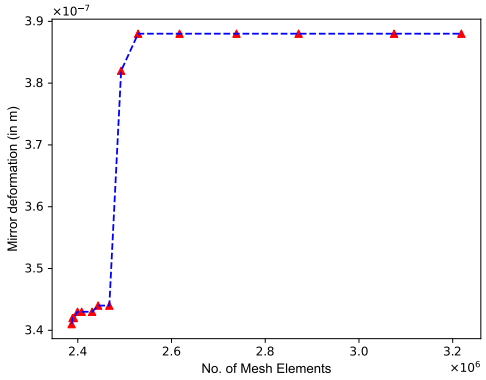

(d) Mesh sensitivity for upper bracket

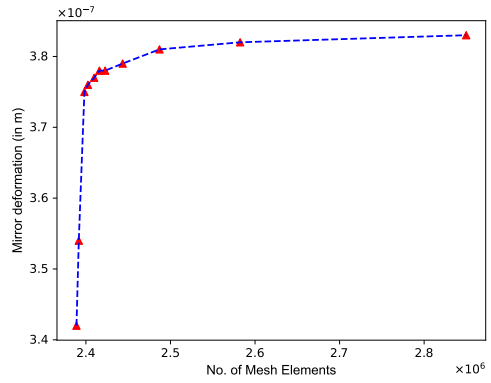

(e) Mesh sensitivity for connecting screws

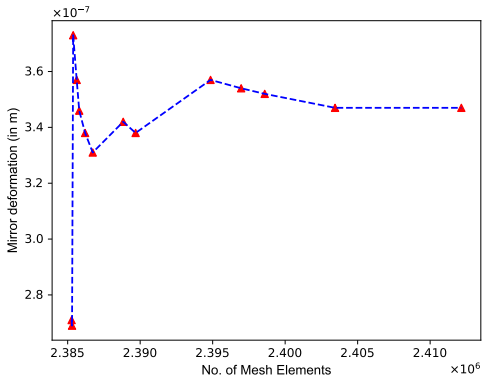

(f) Mesh sensitivity for bracket filler

Figure 3.15: Mesh sensitivity plots for different components of the cavity

To begin with, a reasonable uniform mesh for is considered for all the components. The mesh is optimized by reducing the mesh size for individual components, while keeping the mesh intact for the rest of the model. The plots below show the plateau obtained in the mesh sensitivity curves for different elements. The mesh size optimum for the computation is chosen from the point where the plateau originates. Table 3.8 lists the final mesh sizes used for the analysis.

Table 3.8: Optimum mesh sizes (in mm) for different components of the cavity assembly.

Spacer	Mirror	Lower bracket	Upper bracket	Filler	Screws	Shield base
1.00	1.00	1.10	1.35	0.60	0.50	10.0

3.4.2 Acceleration sensitivity analysis

The acceleration sensitivity analysis is performed on the cavity assembly to characterize its vibration stability. The assembly is subjected to an acceleration of $1g$, in the direction along the cavity axis, and perpendicular to the cavity axis (The cavity is oriented along the z-axis). The acceleration is applied separately in the three orthogonal directions to understand the effect on the cavity and mirror deformations independently. The spacer geometry adopted for the analysis is tapered cylinder (I), as mentioned in the table 3.7. The lower bracket of the mounting structure is a constant feature. Whereas, stability performance for the three different upper bracket designs are analysed. Standard M4 size screws are used to connect the two brackets.

The brackets are assigned the material properties of Duralumin, to provide rigidity in mounting and additionally for due to its low thermal emissivity. The material for the filler which acts as an interface between the upper bracket and spacer is crucial in determining the vibration stability. The acceleration sensitivity is also carried out for different combinations of filler material to determine the appropriate choice.

Fig.3.16 shows acceleration sensitivity curves for different designs of the upper bracket. Three materials were considered for the filler: RTV silicone, Teflon and PEEK. The choice of material for the filler does not show a uniform behaviour across all the upper brackets, but is rather dependent on the design of the bracket. But in general, the vibration stability improves for a filler with higher modulus of rigidity. Hence, PEEK and Teflon is found to be suitable materials for the filler compared to silicone. Teflon is easily available and has good thermal insulation properties. Therefore, the material for the filler is chosen to be Teflon.

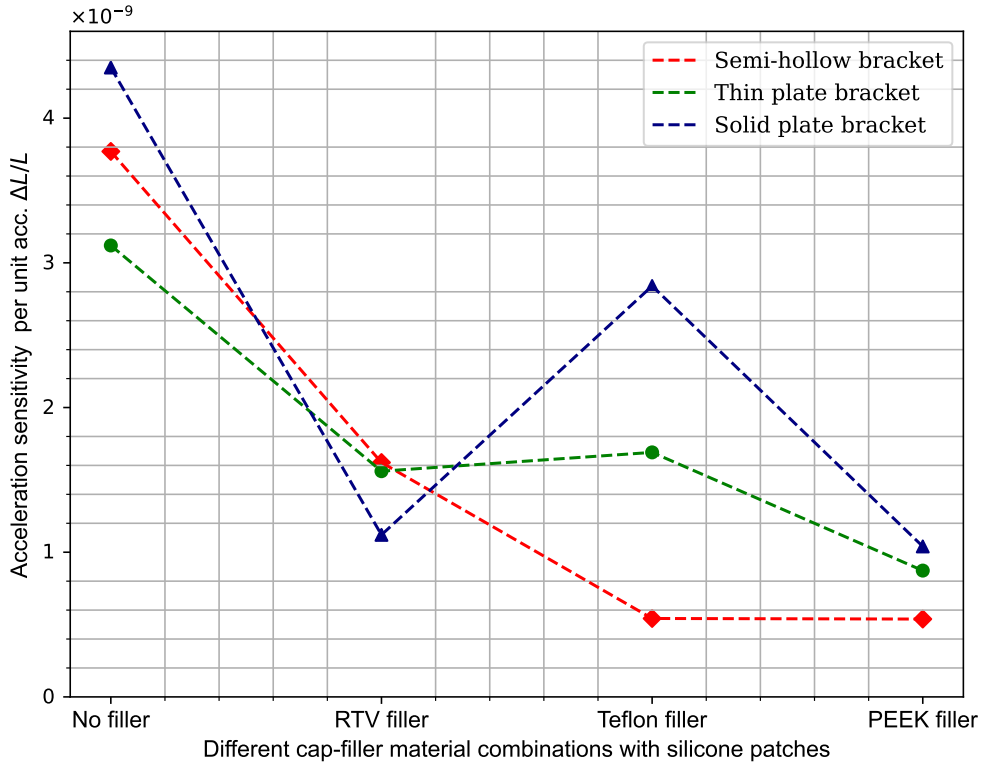

Figure 3.16: Acceleration stability comparison of different top-frame designs, and for material combinations.

The relative change in cavity length causing vibration instability arises due to the non-uniform deformation of the spacer above and below the mid-plane collar, as illustrated in Fig.3.17. When the cavity assembly is accelerated, the forces acting on the cavity at the mounting points differ on the upper and lower patches of the spacer due to the inherent disparity in the upper and lower bracket designs. While the entire spacer collectively displaces downward due to the inertial force, the deformation is larger in the upper half of the spacer compared to the lower half. This difference is influenced both by the design of the upper bracket and the filler material. Filler material of higher shear modulus reduces the effect. The non-uniform spacer deformation is more prominent for solid and thin plate brackets, and is observed to be comparatively lesser for the semi-hollow upper bracket.

Table 3.9: The highest vibration stability offered by upper brackets in $\Delta L/Lg^{-1}$

Solid plate bracket	Semi-hollow bracket	Thin plate bracket
1.04×10^{-9}	$\mathbf{5.38\times10^{-10}}$	8.73×10^{-10}

In an attempt to make the bracket design more uniform, a structure similar to the inverted version of the upper bracket was integrated to the pyramidal lower bracket.

This not only made the mounting bulkier, but offered no significant improvement in the stability. Hence, the simpler version of the lower bracket was retained. The acceleration sensitivity analysis estimates higher vibration stability for the semi-hollow upper bracket design at a value of $\mathbf{5.38{\times}10^{-10}}$.

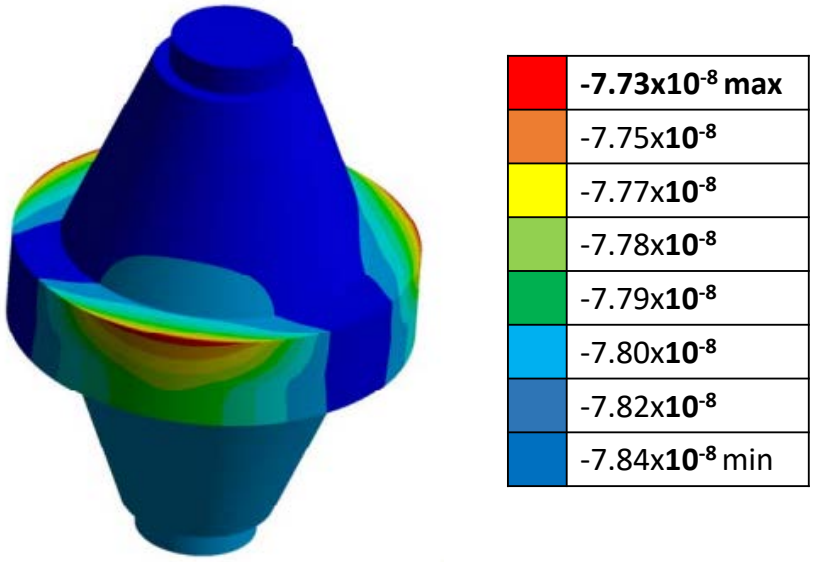

Figure 3.17: The deformation profile of the cavity spacer under constant $1g$ acceleration along cavity axis. The non-uniform deformation in the upper and lower halves (indicated by different shades of blue) of the spacer result in change of cavity length. The region of least deformation (red) occurs around the silicone patches where the cavity is fixed.

The acceleration sensitivity analysis is also performed for the two other optimised spacer geometries in table 3.7, with the bracket that has provided best stability so far: the semi-hollow bracket. However, the stability is not found to be better than the initially considered spacer geometry. The results of the analysis are summarised below:

Table 3.10: Vibration stability of the spacer geometries obtained from table 3.7 with semi-hollow bracket mounting, in units of $\Delta L/Lg^{-1}$.

Sl. no.	Spacer geometry	Filler material	Vibration stability
1.	Tapered cylinder (II)	RTV silicone	$1.96{\times}10^{-9}$
		Teflon	$2.48{\times}10^{-9}$
		PEEK	$5.51{\times}10^{-9}$
2.	Regular cylinder	RTV silicone	$1.22{\times}10^{-9}$
		Teflon	$4.65{\times}10^{-9}$
		PEEK	$3.59{\times}10^{-9}$

3.5 Modal analysis

Modal analysis provides the critical information on the natural resonant modes of the system. The vibration modes could be due to any single component of the assembly or due to the entire assembly itself. In the former case, the structure can be strengthened or re-configured to eliminate the resonant modes. If the modes are due to the assembly, the model may have to be redesigned. Typically, the mechanical vibrations from external environment in the high frequency regime can be suppressed using active vibration table on which the cavity assembly rests. The vibrations in the lower frequency range of 0-100 Hz that cannot be effectively suppressed by vibration tables, are troublesome and needs to be decoupled passively by means of optimizing the design and mounting. The mode shape results play a key role in understanding the nature of resonant modes and addressing the design elements accordingly.

The analysis is performed on all three models of the cavity assembly to identify the dominant vibration modes in each design. The natural frequencies within 100 Hz, if any, are to be strictly eliminated. If not, the resonant modes are tried to be kept as high as possible to achieve maximum decoupling from the external vibration noise. Since there are no moving parts in the system there are no internal vibration sources.

Tables 3.11, 3.12, 3.13 mention the first five natural resonant frequencies for each of the models (with different bracket designs), and for different material combinations. The number of modes considered are such that all the modes <2kHz are included, and the higher modes are ignored. A general trend that is observed in the modal frequencies of the bracket designs for any particular filler material is: $N_{thinplate} < N_{solidplate} \approx N_{semi-hollow}$ uniformly across the modes. Moreover, the modal frequencies are higher for Teflon and PEEK fillers as compared to the silicone filler: $N_{silicone} < N_{Teflon} < N_{PEEK}$. None of the natural frequencies are found to be below 100Hz, with the lowest mode observed for the thin plate bracket with silicone filler at 164.3Hz.

It is noticed that for all the models, irrespective of the upper bracket design or filler material, the mode shapes are more or less similar. Some of the typical mode shapes observed for the cavity assembly at $N = 1$, $N = 3$, and $N = 4$ are represented in Fig.3.18, 3.19, and 3.20) (Mode shape for $N = 2$ is similar to that of $N = 1$). The vibration axis for each of the modes can be determined using the mode shape results in order to analyze their effect on changing the cavity length. The mode shapes are a great tool for visualising the resonant modes of the system.

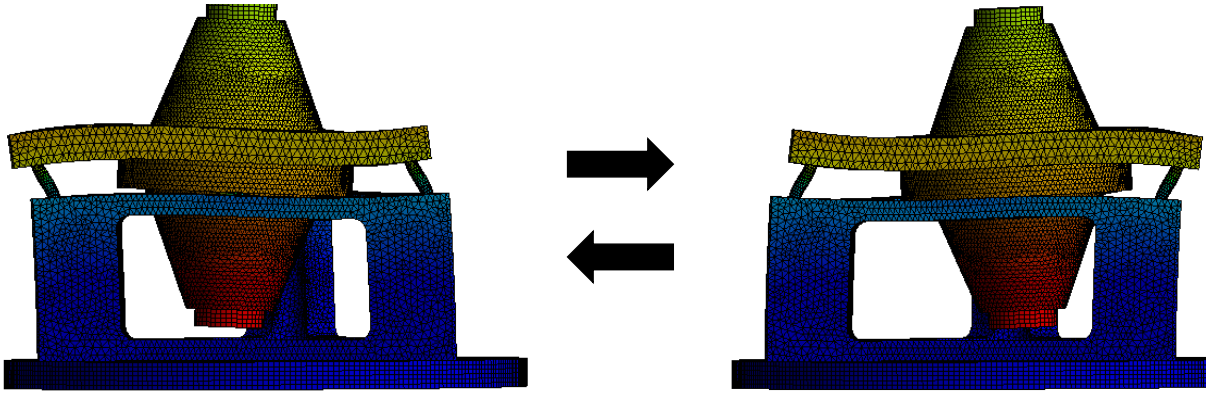

Figure 3.18: $N = 1$ Natural mode shape for the tapered cylinder cavity assembly under vertical mounting with semi-hollow bracket and M4 screws (no external load).

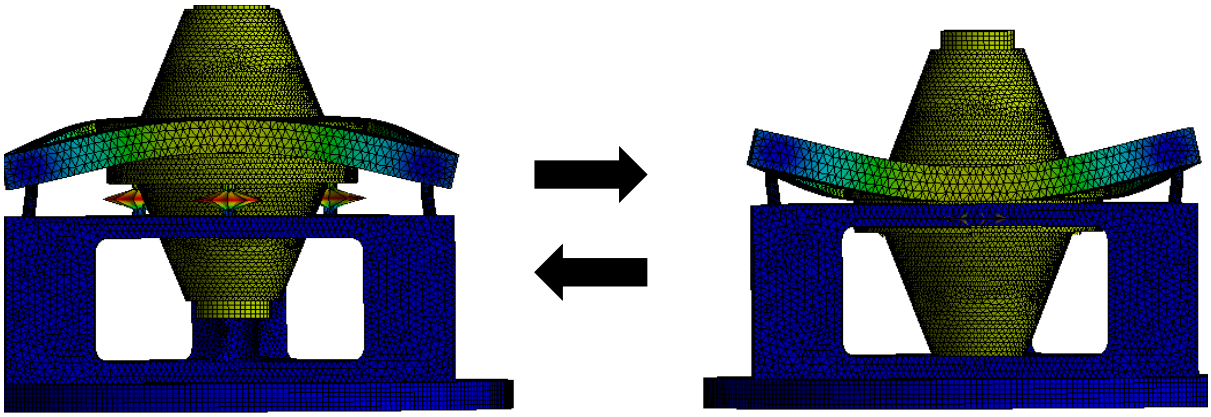

Figure 3.19: $N = 3$ Natural mode shape for the tapered cylinder cavity assembly under vertical mounting with semi-hollow bracket and M4 screws (no external load).

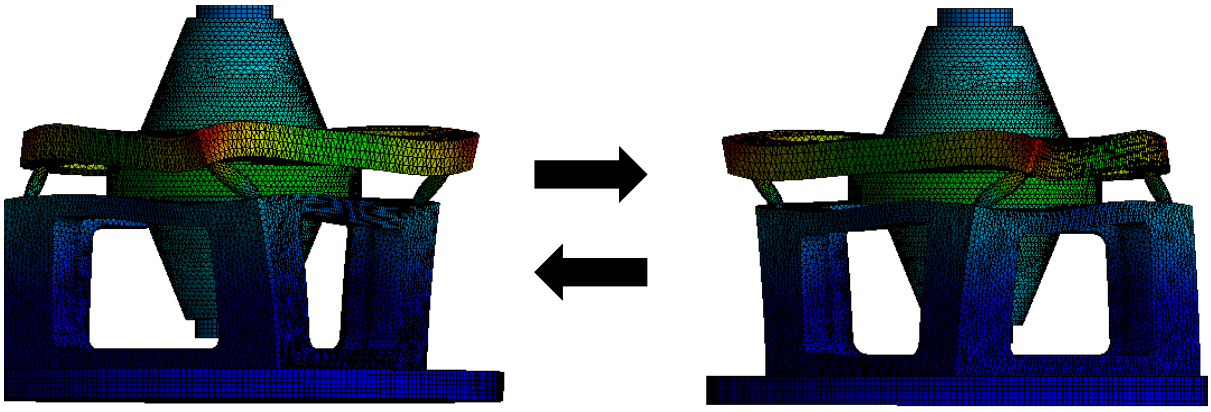

Figure 3.20: $N = 4$ Natural mode shape for the tapered cylinder cavity assembly under vertical mounting with semi-hollow bracket and M4 screws (no external load).

Table 3.11: Modal frequencies (in Hz) for solid bracket assembly (no external load)

Filler material	$N = 1$	$N = 2$	$N = 3$	$N = 4$	$N = 5$
RTV silicone	288.8	291.4	439.9	527.0	1793.7
Teflon	702.4	1029.2	1391.1	1514.6	–
PEEK	710.1	1272.5	1410.5	1960.2	–

Table 3.12: Modal frequencies (in Hz) for semi-hollow bracket assembly (no external load)

Filler material	$N = 1$	$N = 2$	$N = 3$	$N = 4$	$N = 5$
RTV silicone	272.6	285.7	440.3	502.6	1818.2
Teflon	642.2	660.9	1087.8	1554.7	–
PEEK	670.4	712.0	1240.7	1586.1	–

Table 3.13: Modal frequencies (in Hz) for thin bracket assembly (no external load)

Filler material	$N = 1$	$N = 2$	$N = 3$	$N = 4$	$N = 5$
RTV silicone	175.0	188.4	281.2	399.0	1387.7
Teflon	210.4	223.1	374.1	754.8	–
PEEK	216.1	226.8	387.9	763.2	–

The modal shape results reveal that the weakest structure in the mounting assembly are the screws. Initially, standard M4 screws were used for connections. In order to increase the strength, and thereby raise the natural frequency of the assembly, screws of larger diameter are used, namely the M6 and M8 screws. The natural frequencies were observed to increase with the screw size. Additionally, the thicker screws do not degrade the acceleration sensitivity. Hence, the M8 screws were finally opted for the connections in the assembly.

Table 3.14: Modal frequencies for different screw sizes in semi-hollow bracket assembly

Screw size	$N = 1$	$N = 2$	$N = 3$	$N = 4$	$N = 5$
M4 screw	642.2	660.9	1087.8	1554.7	–
M6 screw	877.3	904.2	1339.1	1865.7	–
M8 screw	967.8	1090.0	1498.5	1924.2	–

3.6 Random vibration analysis

In the final stage of analysis, to more accurately understand the response of the cavity against vibrations, random vibration analysis (RVA) is employed. RVA captures the frequency-dependent behaviour of the deformations due to the dispersion in natural vibrations, and the induced response in any system based on its vibration modes and resonances. From the results of section 3.4.2 and 3.5, two of the design parameters in the mounting structure are fixed: *Teflon* material for the filler, and $M8$ size screws for connection. Once again, all the three designs of the bracket are considered for testing the frequency response of the deformations in the cavity mirror due to vibrations, which ultimately cause the change in cavity length during the operation.

To simulate the typical vibration environment experienced by the transportable cavity, the pre-existing local ground vibration data is obtained from the laboratory (Fig.3.21). The seismic vibrations data act as the input PSD for the random vibration analysis, transmitted to the body through the fixed supports points. Unlike the acceleration sensitivity analysis, where the direction of the deformations of the individual mirrors are known, one cannot characterize the vibration stability in terms of $\Delta L/Lg^{-1}$ in RVA. The input function in RVA is a spectral distribution, as a result of which the output parameter, such as the deformation, is also expressed in terms of its spectral density or response PSD. Due to the stochastic nature of the process, the deformations are rather averaged over an interval of time, and hence the directionality is lost. This is the drawback in random vibration analysis.

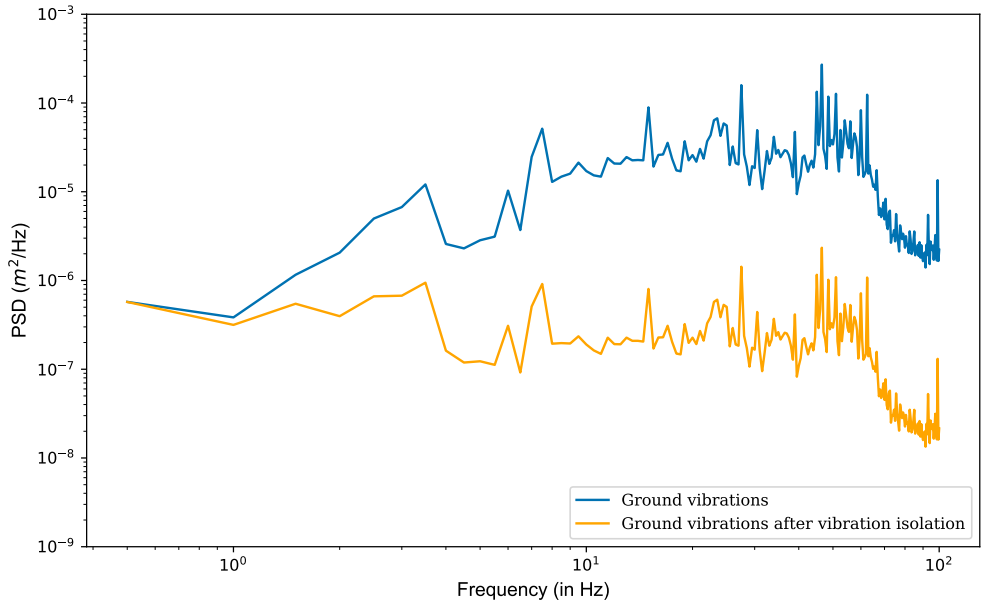

Figure 3.21: Seismic vibrations data for PQM lab, IUCAA

Since the relative deformation in the cavity length cannot be determined, the deformations in the individual mirrors can be studied and compared at best. Fig.3.22 shows the deformations at the centre of the two mirrors of the cavity mounted using different brackets without any vibration isolation. It can be observed that the response PSD curves for the mirror deformations corresponding to any particular model pretty much overlap. Although it cannot be known if the deformations are in-phase, the magnitude of the deformations are found to be approximately equal. Further, the deformation levels are lower in solid and semi-hollow brackets compared to the thin bracket. These observation reinforces the previous results obtained in section 3.4.2. The RMS values of the mirror deformations obtained from area under the response PSD curves are compared in table.

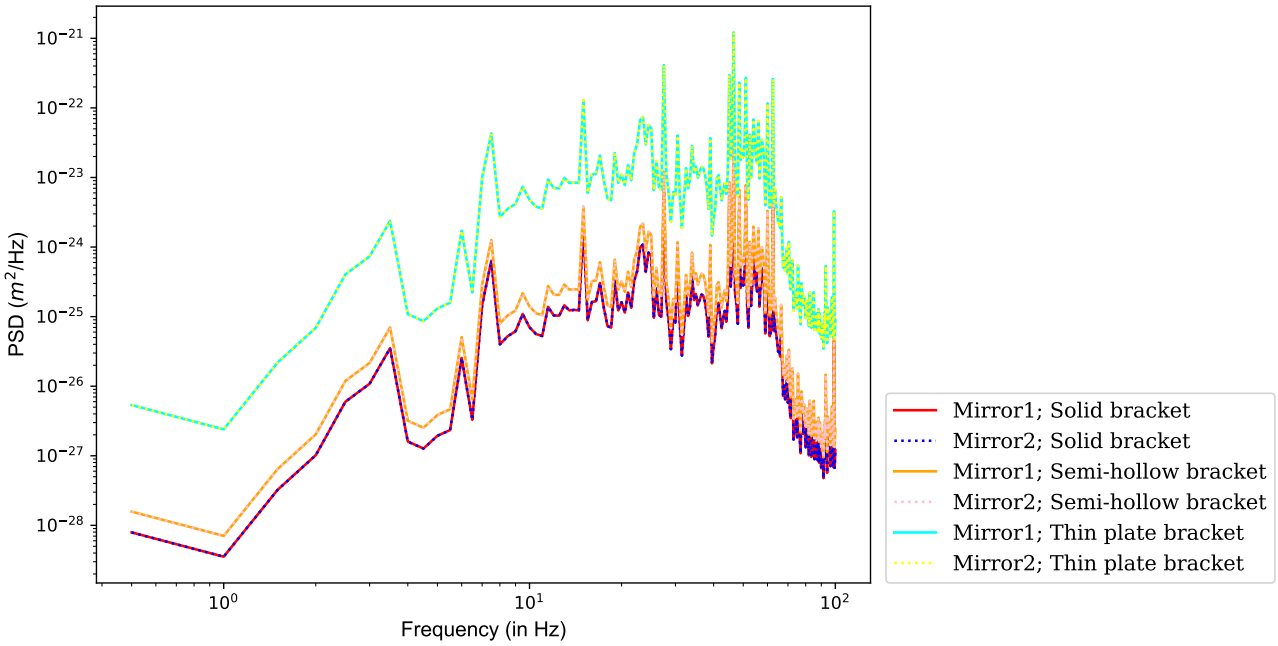

Figure 3.22: Comparing the deformations due to seismic vibrations at the mirror centre for both mirrors (mirror 1 and mirror 2) in the cavity, for different mounting bracket designs (with Teflon fillers and M8 size screws). No vibration isolation is provided to the system.

Table 3.15: The RMS values for deformations at the centre of the mirrors for cavities with different brackets for mounting.

	Solid bracket	Semi-hollow bracket	Thin bracket
RMS Deformation of Mirror 1 (in m)	4.84×10^{-12}	6.83×10^{-12}	4.01×10^{-11}
RMS Deformation of Mirror 2 (in m)	4.83×10^{-12}	6.82×10^{-12}	4.01×10^{-11}

The cavity mounting design with semi-hollow bracket gives competent results in all the methods used to characterize the vibration stability in this thesis. Hence, the semi-hollow bracket design with Teflon filler and M8 screws are finalised for the mounting of the transportable cavity.

The fractional frequency stability of the transportable cavity with finalised mounting is estimated. As discussed in section 2.6.3, the vibration stability obtained through acceleration sensitivity analysis in terms of $\Delta L/Lg^{-1}$ can be scaled to the magnitude of actual vibrations experienced by the cavity, as represented by the ground vibrations PSD in Fig.3.21. Until now, the frequency instability $\frac{\Delta\nu}{\nu}$ due to relative change in cavity length $\Delta L/L$ is considered. The effect of the misalignment caused in the cavity due to vibrations adds to the frequency noise through power re-distribution in HOMs. Although this effect is negligible in comparison to the effect due to change in cavity length, the final fractional frequency stability estimation comprises of both the noise terms. The detailed analysis of the calculation to combine the frequency noise due to $\Delta L/L$ and misalignment is beyond the scope of this thesis. The fractional frequency stability due to vibrations with and without the use of active vibration isolation is plotted in the Fig.3.23.

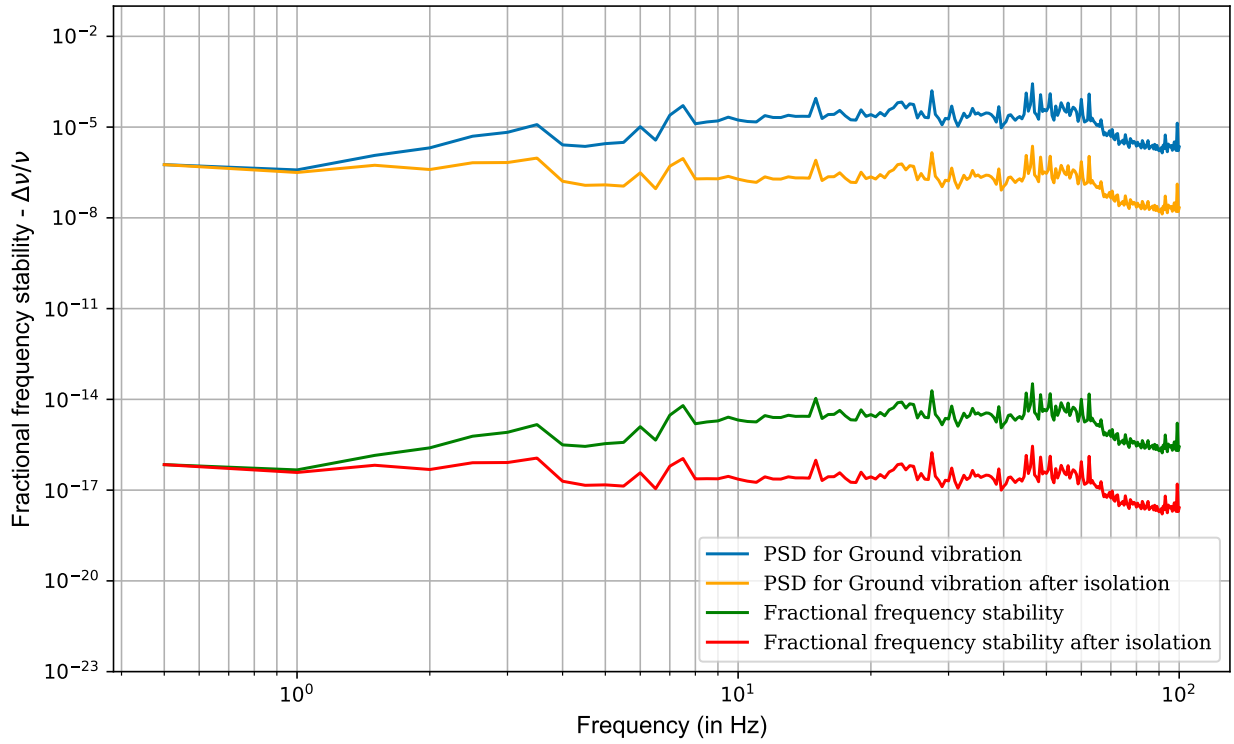

Figure 3.23: The fractional frequency stability for the tapered cylinder transportable cavity with the mounting designed in this thesis.

The fractional frequency stability attained is: $\frac{\Delta\nu}{\nu} = \mathbf{1.55{\times}10^{-15}}$ at 1Hz (after isolation).

Chapter 4

Conclusion and outlook

In this thesis, the designing of a reference optical cavity that is transportable and specialized for out of the lab applications is carried out. Due to the vibration stability limitations in portable reference cavities, the emphasis has been on mitigating the frequency noise developed due to mechanical vibrations of the system. Various structural aspects like spacer geometry, support framework, mounting and assembly are explored in order to make the cavity robust to vibration noise. Rigorous quantitative analysis and finite element simulations are performed to verify the designs and characterize their stability.

In order to keep the transportable cavity compact, a small length-scale of 105.5 mm was chosen after the optimization of length for reduced noise from cavity higher order transverse modes. A tapered cylinder geometry is chosen for the cavity due to its zero-crossing property in deformations for vibration stability, and also due to its smaller volume. The mounting scheme for the cavity is adopted partially similar to one followed in [44]. However, a novel mounting structure based on two monolithic brackets, connected by screws is conceptualised. The stability of the designed mounting is verified using three different methods of vibration stability analysis. Out of three different designs for the bracket structure considered, the semi-hollow bracket with least acceleration sensitivity is chosen. The vibration stability in terms of $\Delta L/Lg^{-1}$ is estimated at 5.38×10^{-10} for the semi-hollow bracket design.

Further, modal analysis identifies the natural resonance modes of the cavity assembly. The design is optimised by using screws of larger diameter in order to increase the modal frequency of the cavity assembly, which enhances its stability. Finally, the random vibration analysis was carried out to understand the frequency dependent deformation response in the cavity. The analysis confirms the magnitude of the deformation of individual mirrors to lie in the same range, which could maintain the cavity relative length stability at a very high degree. The final fractional frequency stability of the cavity due to vibrations with active isolation turns out to be $\mathbf{1.55\times10^{-15}}$ at 1Hz.

The methods used for analysis in this work are some of the standard procedures implemented world-wide to characterize the stability of transportable cavities. However, these methods have some limitations. One of the main limitations is the tolerances incurred during the process of machining and assembly. In simulations, the designs are simplified and boundary conditions defined ideally to estimate the required stability, and also to optimize simulations and computational time. Practically, the machining process involves uncertainties and tolerances for different parameters at different scales. Incorporating all the nuances is not only difficult but can also be very time consuming. The stability characterization of the presented design along with its accompanying tolerances is yet to be carried out.

Dealing with random vibrations in simulations is non-trivial. The fractional frequency stability estimated for the cavity in the thesis is obtained through linear scaling of the vibration stability achieved at $1g$ acceleration to the magnitude of acceleration of actual vibrations. The estimation regards the frequency dependence of the magnitude of acceleration experienced by the cavity, but it does so by considering each frequency separately. In reality, random vibrations are made of several frequencies combined together. While the effect of individual frequencies can be studied on the system, analysing the combined effect of all the frequencies involved to obtain a meaningful result is still an open problem. In future, FE simulations that use innovative methods like Forced Vibration analysis, as described in [10], to characterize the vibration stability will be explored.

That said, within the reasonable limit of error, the methodology adopted here in determining the stability estimates the vibration stability to a very good extent. Moreover, multiple approaches are implemented to verify and optimize the design to meet the needs of the transportable cavity. The cavity thus obtained is compact, lightweight, robust and can withstand the vibration environment in non-laboratory conditions. The best transportable cavities designed till date have achieved a vibration stability of $2.45(3)\times10^{-11}$ [42], 4×10^{-11} [45], $3.0(3)\times10^{-12}$ [49] in terms of $\Delta L/Lg^{-1}$. Compared to the available transportable cavities, the stability achieved through simulations for the novel mounting design presented in this work at a value of $\mathbf{5.38\times10^{-10}}$ may not be exceptional, but very well serves the purpose of a transportable cavity. This work provides the baseline analysis for tapered cylinder geometry as a candidate for room-temperature reference optical cavities, for which more innovative and stable support structures can be contemplated. The completion of the transportable cavity design hereon proceeds to the thermal stability analysis, by assimilating the cavity-mounting assembly with thermal shields and active or passive temperature control features. The design of the vacuum chamber for high vacuum, along with integration of laser source and servo electronics makes the transportable

cavity ready for application.

The research and demand for transportable cavities is ever-growing. With new stability and SWaP requirements for cavities emerging due to various applications of academic interest, like gravitational wave detection, precision metrology, and real-world applications, like low-noise RADAR, faster and accurate communication and navigation, the innovations in the field of transportable cavities will continue to flourish. Several companies have already established themselves as experts in manufacturing the cavities or cavity elements for research and commercial use. New methods and research continue to pour from laboratories across the world, with the next generation cavities aiming at fully functional cryogenic [69] and space-grade cavities [70]. The use of new analytical and computational methods to determine the cavity stability are also widely explored, like the one on use of Data Learning to optimize the cavity design described in [71]. The efforts made in this work is towards developing a transportable ultra-stable laser system for high precision portable optical clocks. The future work will focus on completing the cavity design, and exploring ways to minimize the effect of noises to obtain a fully integrated and functional ultra-stable transportable room-temperature reference cavity.

Bibliography

1. Liu, J. *et al.* A compact sub-hertz linewidth Fabry Perot cavity frequency stabilized laser for space application. *Optics & Laser Technology* **136,** 106777 (2021).
2. Lasers, S. *Fabry-Perot Cavities* `https://stablelasers.com/fabry-perot-cavities/`. 2024.
3. Álvarez, M. D. & Álvarez, M. D. Near-Unstable Cavities for Future Gravitational Wave Detectors. *Optical Cavities for Optical Atomic Clocks, Atom Interferometry and Gravitational-Wave Detection,* 191–211 (2019).
4. Born, M. & Wolf, E. *Principles of optics: electromagnetic theory of propagation, interference and diffraction of light* (Elsevier, 2013).
5. Sánchez-Soto, L. L., Monzón, J. J. & Leuchs, G. The many facets of the Fabry–Perot. *European Journal of Physics* **37,** 064001 (2016).
6. Gong, Y., Li, B.-c. & Han, Y.-l. Optical feedback cavity ring-down technique for accurate measurement of ultra-high reflectivity. *Applied Physics B* **93,** 355–360 (2008).
7. Ismail, N., Kores, C. C., Geskus, D. & Pollnau, M. Fabry-Pérot resonator: spectral line shapes, generic and related Airy distributions, linewidths, finesses, and performance at low or frequency-dependent reflectivity. *Optics express* **24,** 16366–16389 (2016).
8. Drever, R. W. *et al.* Laser phase and frequency stabilization using an optical resonator. *Applied Physics B* **31,** 97–105 (1983).
9. Black, E. D. An introduction to Pound–Drever–Hall laser frequency stabilization. *American journal of physics* **69,** 79–87 (2001).
10. Banerjee, S. *et al.* Modelling and design of ultra-high stable Fabry–Pérot cavity. *International Journal of Mechanical Sciences* **250,** 108299 (2023).
11. Alnis, J., Matveev, A., Kolachevsky, N., Udem, T. & Hänsch, T. Subhertz linewidth diode lasers by stabilization to vibrationally and thermally compensated ultralow-expansion glass Fabry-Pérot cavities. *Physical Review A* **77,** 053809 (2008).

12. Ludlow, A. D. *et al.* Compact, thermal-noise-limited optical cavity for diode laser stabilization at 1× 10- 15. *Optics Letters* **32,** 641–643 (2007).

13. Young, B., Cruz, F., Itano, W. & Bergquist, J. Visible lasers with subhertz linewidths. *Physical Review Letters* **82,** 3799 (1999).

14. Jiang, Y. *et al.* Making optical atomic clocks more stable with 10- 16-level laser stabilization. *Nature Photonics* **5,** 158–161 (2011).

15. Riou, I. *et al.* A marginally stable optical resonator for enhanced atom interferometry. *Journal of Physics B: Atomic, Molecular and Optical Physics* **50,** 155002 (2017).

16. Zalivako, I. V. *et al.* Compact ultrastable laser system for spectroscopy of 2S1/2→ 2D3/2 quadrupole transition in 171Yb+ ion. *Quantum Electronics* **50,** 850 (2020).

17. Giunta, M. *et al.* Compact and ultrastable photonic microwave oscillator. *Optics Letters* **45,** 1140–1143 (2020).

18. Chen, Q., Magoulakis, E. & Schiller, S. High-sensitivity crossed-resonator laser apparatus for improved tests of Lorentz invariance and of space-time fluctuations. *Physical Review D* **93,** 022003 (2016).

19. Wcisło, P. *et al.* New bounds on dark matter coupling from a global network of optical atomic clocks. *Science Advances* **4,** eaau4869 (2018).

20. Hobson, R. *et al.* A strontium optical lattice clock with 1× 10- 17 uncertainty and measurement of its absolute frequency. *Metrologia* **57,** 065026 (2020).

21. Herrmann, S. *et al.* Rotating optical cavity experiment testing Lorentz invariance at the 10- 17 level. *Physical Review D* **80,** 105011 (2009).

22. Zhadnov, N. *et al.* 48-cm-long room-temperature cavities in vertical and horizontal orientations for Sr optical clock. *Applied Optics* **60,** 9151–9159 (2021).

23. Jin, L. *et al.* Laser frequency instability of 2× 10- 16 by stabilizing to 30-cm-long Fabry-Pérot cavities at 578 nm. *Optics Express* **26,** 18699–18707 (2018).

24. Robinson, J. M. *et al.* Crystalline optical cavity at 4 K with thermal-noise-limited instability and ultralow drift. *Optica* **6,** 240–243 (2019).

25. Matei, D. *et al. A second generation of low thermal noise cryogenic silicon resonators* in *Journal of Physics: Conference Series* **723** (2016), 012031.

26. Zhang, W. *et al.* Ultrastable silicon cavity in a continuously operating closed-cycle cryostat at 4 K. *Physical review letters* **119,** 243601 (2017).

27. Kedar, D. *et al.* Frequency stability of cryogenic silicon cavities with semiconductor crystalline coatings. *Optica* **10,** 464–470 (2023).

28. Koller, S. *et al.* Transportable optical lattice clock with 7× 10- 17 uncertainty. *Physical Review Letters* **118,** 073601 (2017).

29. Cao, J. *et al.* A compact, transportable single-ion optical clock with 7.8× 10- 17 systematic uncertainty. *Applied Physics B* **123,** 1–9 (2017).

30. Bongs, K. *et al.* Development of a strontium optical lattice clock for the SOC mission on the ISS. *Comptes Rendus Physique* **16,** 553–564 (2015).

31. Fortier, T. M. *et al.* Generation of ultrastable microwaves via optical frequency division. *Nature Photonics* **5,** 425–429 (2011).

32. Liu, Y. *et al.* Experimental twin-field quantum key distribution over 1000 km fiber distance. *Physical Review Letters* **130,** 210801 (2023).

33. Giorgi, G. *et al.* Advanced technologies for satellite navigation and geodesy. *Advances in Space Research* **64,** 1256–1273 (2019).

34. Numata, K. *et al. Laser system development for the LISA (Laser Interferometer Space Antenna) mission* in *Solid State Lasers XXVIII: Technology and Devices* **10896** (2019), 231–237.

35. Nicklaus, K. *et al. High stability laser for next generation gravity missions* in *International Conference on Space Optics—ICSO 2014* **10563** (2017), 808–815.

36. Gürlebeck, N. *et al.* BOOST: a satellite mission to test Lorentz invariance using high-performance optical frequency references. *Physical Review D* **97,** 124051 (2018).

37. Acef, O., Clairon, A. & Du Burck, F. *Nd: YAG laser frequency stabilized for space applications* in *International Conference on Space Optics—ICSO 2010* **10565** (2019), 956–961.

38. Häfner, S. *et al.* 8× 10- 17 fractional laser frequency instability with a long room-temperature cavity. *Optics Letters* **40,** 2112–2115 (2015).

39. Xiao, R., Xu, Y., Wang, Y., Sun, H. & Chen, Q. Transportable 30 cm optical cavity based ultrastable lasers with beating instability of 2× 10-16. *Applied Physics B* **128,** 220 (2022).

40. Tao, B.-K. & Chen, Q.-F. A vibration-insensitive-cavity design holds impact of higher than 100 g 100 g. *Applied Physics B* **124,** 1–6 (2018).

41. Leibrandt, D. R. *et al.* Spherical reference cavities for frequency stabilization of lasers in non-laboratory environments. *Optics Express* **19,** 3471–3482 (2011).

42. Webster, S. & Gill, P. Force-insensitive optical cavity. *Optics Letters* **36,** 3572–3574 (2011).

43. Zhao, P. *et al.* A spaceborne mounting method for fixing a cubic Fabry–Pérot cavity in ultra-stable lasers. *Applied Sciences* **12,** 12763 (2022).

44. Parker, B. *et al.* Transportable cavity-stabilized laser system for optical carrier frequency transmission experiments. *Applied Optics* **53,** 8157–8166 (2014).

45. Argence, B. *et al.* Prototype of an ultra-stable optical cavity for space applications. *Optics Express* **20,** 25409–25420 (2012).

46. Świerad, D. *et al.* Ultra-stable clock laser system development towards space applications. *Scientific Reports* **6,** 33973 (2016).

47. Davila-Rodriguez, J. *et al.* Compact, thermal-noise-limited reference cavity for ultra-low-noise microwave generation. *Optics Letters* **42,** 1277–1280 (2017).

48. Chen, X. *et al.* Laser frequency instability of 6× 10- 16 using 10-cm-long cavities on a cubic spacer. *Chinese Optics Letters* **18,** 030201 (2020).

49. Herbers, S. *et al.* Transportable clock laser system with an instability of 1.6× 10-16. *Optics Letters* **47,** 5441–5444 (2022).

50. Didier, A. *et al.* Ultracompact reference ultralow expansion glass cavity. *Applied Optics* **57,** 6470–6473 (2018).

51. Zhao, W. *et al.* Design of a transportable miniaturized optical reference cavity with flexibly tunable thermal expansion properties. *Frontiers in Physics* **10,** 1080196 (2023).

52. Webster, S., Oxborrow, M., Pugla, S., Millo, J. & Gill, P. Thermal-noise-limited optical cavity. *Physical Review A* **77,** 033847 (2008).

53. Sanjuan, J. *et al.* Long-term stable optical cavity for special relativity tests in space. *Optics Express* **27,** 36206–36220 (2019).

54. Chen, Q.-F. *et al.* A compact, robust, and transportable ultra-stable laser with a fractional frequency instability of 1× 10- 15. *Review of Scientific Instruments* **85** (2014).

55. Chen, L. *et al.* Theoretical and experimental study on vibration sensitivity of cubic cavity for space applications. *Optics & Laser Technology* **158,** 108915 (2023).

56. Folkner, W. *et al. Laser frequency stabilization for GRACE-II* (Pasadena, CA: Jet Propulsion Laboratory, National Aeronautics and Space ..., 2010).

57. Li, Z., Ma, W., Yang, W., Wang, Y. & Zheng, Y. Reduction of zero baseline drift of the Pound–Drever–Hall error signal with a wedged electro-optical crystal for squeezed state generation. *Optics Letters* **41,** 3331–3334 (2016).

58. Liu, Y. & Daum, P. H. Relationship of refractive index to mass density and self-consistency of mixing rules for multicomponent mixtures like ambient aerosols. *Journal of Aerosol Science* **39,** 974–986 (2008).

59. Callen, H. B. & Greene, R. F. On a theorem of irreversible thermodynamics. *Physical Review* **86,** 702 (1952).

60. Numata, K., Kemery, A. & Camp, J. Thermal-noise limit in the frequency stabilization of lasers with rigid cavities. *Physical review letters* **93,** 250602 (2004).

61. Kessler, T., Legero, T. & Sterr, U. Thermal noise in optical cavities revisited. *JOSA B* **29,** 178–184 (2012).

62. Amairi, S. *et al.* Reducing the effect of thermal noise in optical cavities. *Applied Physics B* **113,** 233–242 (2013).

63. Cole, G. D., Gröblacher, S., Gugler, K., Gigan, S. & Aspelmeyer, M. Monocrystalline AlxGa1- xAs heterostructures for high-reflectivity high-Q micromechanical resonators in the megahertz regime. *Applied Physics Letters* **92** (2008).

64. ANSYS. *Materials Data for Simulation* `https://www.ansys.com/en-in/products/materials/materials-data-for-simulation`. 2024.

65. Robinson, J. M. *et al.* Thermal noise and mechanical loss of SiO 2/Ta 2 O 5 optical coatings at cryogenic temperatures. *Optics Letters* **46,** 592–595 (2021).

66. Qian, Y., Xie, Y., Jia, J. & Zhang, L. Design of active vibration isolation controller with disturbance observer-based linear quadratic regulator for optical reference cavities. *Sensors* **23,** 302 (2022).

67. Jiao, D. *et al.* Highly vibration-resistant sub-Hertz ultra-stable laser passing over 1700 km transport test. *Infrared Physics & Technology* **130,** 104608 (2023).

68. Araya, A. *et al.* Optical mode cleaner with suspended mirrors. *Applied optics* **36,** 1446–1453 (1997).

69. Wang, W.-W. *et al.* Design and realization of a 3-K cryostat for a 10-cm ultrastable silicon cavity. *Frontiers in Physics* **11,** 1176783 (2023).

70. Guo, X. *et al.* An automatic frequency stabilized laser with hertz-level linewidth. *Optics & Laser Technology* **145,** 107498 (2022).

71. Zhao, H. *et al.* Multi-Physics and Multi-Objective Optimization for Fixing Cubic Fabry–Pérot Cavities Based on Data Learning. *Applied Sciences* **13,** 13115 (2023).